Self-Assembled Colloidal Gold Nanoparticles as Substrates for Plasmon Enhanced Fluorescence

Oscar F. Silvestre[a,b#], Anish Rao[a#], Luis M. Liz-Marzán[a,b,c*]

[a] *Center for Cooperative Research in Biomaterials (CIC biomaGUNE), Basque Research and Technology Alliance (BRTA), Paseo de Miramón 182, 20014 Donostia-San Sebastián, Spain.*
[b] *Centro de Investigación Biomédica en Red, Bioingeniería, Biomateriales y Nanomedicina (CIBER-BBN), Paseo de Miramón 182, 20014 Donostia-San Sebastián, Spain.*
[c] *Iberbasque, 43009 Bilbao, Spain.*

# these authors contributed equally to this work.
*corresponding author

Abstract

Decades of intense research in the field of nanoscience have led to the ability to produce nanoparticles (NPs) with controlled composition, shape, and size. One of the next key challenges is the self-assembly of appropriate NP building blocks into larger systems to obtain micro- or macroscale materials. To achieve this, self-assembly protocols must not only produce high-quality structures, but also deliver the assemblies of interest to desired locations on a substrate. In this review, we discuss different self-assembly strategies, focusing on colloidal gold NPs and applications as plasmon-enhanced fluorescence (PEF) platforms. These plasmonic substrates have been used for biosensing and cell imaging, based on the enhancement of fluorescent emitters, and applied to improve the emission efficiency of luminescent NPs. It is important to note that higher fluorescence enhancement relies on precise control of the location of gold NPs and fluorescent emitters on the plasmonic substrate. Despite the diversity of available self-assembly strategies, many of them provide similar levels of structural control over the placement of gold NPs on the substrate. To highlight this, we have organized the discussion according to strategies that result in similar degrees of structural control over the placement of gold NPs and its associated PEF effect.

Keywords: *self-assembly on a substrate, plasmon enhanced fluorescence, gold nanoparticles, surface plasmons*

1. Introduction

Designing and synthesizing materials with properties tailored for applications in various fields, ranging from wearable bio-integrated sensors (Gao et al., 2016; D. H. Kim et al., 2012), electronics (Talapin & Murray, 2005; S. Wang et al., 2018; X. Zhao et al., 2021), energy storage devices (Aricò et al., 2005; Pomerantseva et al., 2019), catalysis (Daniel & Astruc, 2004), displays (S. F. Liu et al., 2022; Y. Wang et al., 2017), etc. is one of the key promises of materials science. In this direction, multiple strategies have been developed toward the bottom-up assembly of nanoscale building blocks into the anticipated architecture (Boles et al., 2016; Hueckel et al., 2020, 2021; M. S. Lee et al., 2022; Macfarlane, 2021; Rao et al., 2022; Talapin et al., 2015). The key variational principle to meet our diverse material demands exploits the size, shape, surface chemistry and composition dependence of the optoelectronic properties of nanomaterials, which can subsequently be self-assembled into arbitrary structures to obtain macroscopic devices with the properties of interest. Self-assembly is the science of things that form on their own (Pelesko et al., 2007). More precisely, it can be defined as the spontaneous formation of an organized structure from discrete building blocks through stochastic processes (Pelesko et al., 2007). Self-assembly processes are ideally reversible and can be controlled by an appropriate design of the building blocks, their environment and interparticle interactions (Bishop et al., 2009; Pelesko et al., 2007). Decades of intense research have resulted in the ability to produce nanomaterial building blocks of arbitrary compositions, shapes and sizes, with ever-improved monodispersity, yield, and large-scale production. The next key challenge involves using nanoparticles (NPs) with selected properties and craft micro- or macroscale materials therefrom. Meeting this challenge is at the heart of bottom-up assembly protocols. These protocols are in stark contrast to top-down fabrication methodologies, and can oftentimes help realize structures that would be prohibitively time consuming from purely top-down protocols (Figure 1a).

It is important to mention that, some of the most common outcomes at the heart of NP self-assembly are products like colloidal molecules (Yi et al., 2020), NP supercrystals (Kalsin et al., 2006; Scarabelli et al., 2017, 2021), mouldable or plastic NP aggregates (Klajn et al., 2007), dynamic reactors (H. Zhao et al., 2016), sensors (García-Lojo et al., 2019; Grzelczak et al., 2019) etc., each of which can be used for different applications. However, it should be noted that each of these outcomes allows different levels of structural control over the final architecture. For instance, an impressive nano- or angstrom-level control can be achieved in NP supercrystals, whereas mouldable NP inks can be used to control the final structure at the micro- or macroscale (Klajn et al., 2007; Y. Wang et al., 2017). The choice of structural features should thus be made on the basis of the expected set of functions. For instance, organized cavities can be used for sensing and catalytic applications (Udayabhaskararao et al., 2017; H. Zhao et al., 2016), whereas control over microstructures enables the development of materials for photonic and mechanical applications (García-Astrain et al., 2020; M. S. Lee et al., 2022; Santos et al., 2021). Despite the excellent progress made towards the synthesis and assembly of NPs, they have found limited use in large scale industrial applications so far. The key reasons for this latent potential may become apparent by benchmarking the outcomes of self-assembly processes against conventional top-down fabrication protocols. However, additional progress is required in the field NP self-assembly to obtain structures of arbitrary complexity on a variety of substrates. For self-assembly to meet these demands, not only the

nanoscale control over NPs should be perfected, but also their further processing and deposition onto desired places on the substrates of choice (Figure 1b,c).

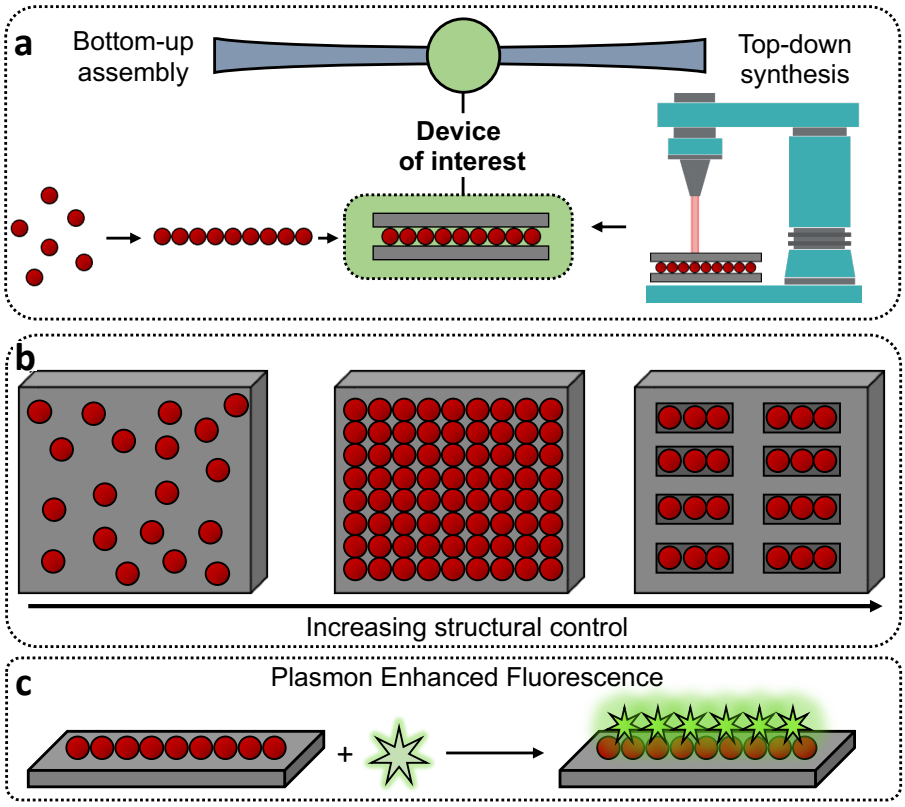

Figure 1. Bottom-up material synthesis with NPs and their self-assemblies. a) Schematics illustrating the formation of a device of interest using two different methods, i.e. top-down and bottom-up self-assembly. **b)** Schematic showing the use of NPs for assembly onto a substrate with increasing level of structural control. **c)** Schematic illustration showing the use of plasmonic substrates as plasmon enhanced fluorescence platforms.

In the present review, we aim to take stock of different protocols for self-assembly on substrates that can help in the formation of next-generation complex matter. For the purposes of the present review, we limit our discussion to the developments made in the context of the plasmon-enhanced fluorescence (PEF). In the literature, several studies have alternatively termed this phenomenon as surface-enhanced fluorescence (SEF) (Fort & Grésillon, 2007; Moskovits, 1985), or metal-enhanced fluorescence (MEF) (Geddes & Lakowicz, 2002; Lakowicz et al., 2008). For the sake of clarity, we use the term plasmon-enhanced fluorescence (PEF) (Bauch et al., 2014; Dong et al., 2015; J. F. Li et al., 2017), while reviewing the self-assembly strategies and applications of colloidal gold nanoparticles (AuNPs) on substrates as PEF platforms (Figure 1c).

The optical properties of plasmonic metal NPs are mainly dictated by the coherent oscillations of their conduction electrons at the metal-dielectric interface, stimulated by an incident electromagnetic radiation (Pelton et al., 2008). Such coherent charge-density oscillations are called localized surface plasmon resonances (LSPR), and result in the localization of light at the nanoscale, generating large local enhancement of the electromagnetic field (Pelton et al., 2008). PEF exploits the use of these plasmonic NPs or nanostructures to alter the excitation and emission rates, radiation patterns, quantum yield, and photostability of different emitters

(Semeniak et al., 2022). The intense local electromagnetic fields generated at the NP surface can increase not only the excitation rate of the emitter, but also its emission due to the increased local density of states, and higher probability of transition from the excited to the ground state (J. F. Li et al., 2017; Semeniak et al., 2022). Several factors influencing the interactions between plasmonic NPs and emitters have been studied, including the overlap between the LSPR of the plasmonic NP and the absorption/emission bands of the emitter, and the distance separating the two (J. F. Li et al., 2017; Semeniak et al., 2022). In this respect, a decrease in the distance between the plasmonic NP and the emitter results in a continuous transition from fluorescence enhancement to the quenching effect, due to energy transfer from the excited emitter to the metal at smaller interparticle distances (Anger et al., 2006; Asian et al., 2004). Anger et al. claimed that fluorescence enhancement reaches maximum when the emitter is located at a distance of 5 nm from the metal surface, whereas quenching would occur at lower distances (Anger et al., 2006). Overall, the use of suitable plasmonic NPs, coupled with appropriate separation distances, results in an enhancement of the emission intensity by several orders of magnitude, as well as a reduction of the fluorescence lifetimes (Dong et al., 2015; Joyce et al., 2020; Semeniak et al., 2022).

Fluorescence is widely used in optical imaging and biosensing platforms, such as immunoassays, where target biomarkers are detected through binding fluorescently labelled antibodies and the signal depends on the amount of biomarker present in the sample. However, low concentrations of biomarkers may not be readily detected by standard instruments, so PEF provides a clear advantage at increasing assay sensitivity with the reduction of biomarker detection limits, which translates into an improvement in disease diagnosis (Bauch et al., 2014; Joyce et al., 2020; Semeniak et al., 2022). PEF also offers the possibility of increasing the emission intensity of luminescent NPs. Namely, upconverting nanoparticles (UCNPs) absorb low-energy light and re-emit light with higher energy, which is interesting for bioimaging, as well as other fields such as solar energy conversion and display technologies. However, UCNPs suffer from low emission efficiency (Dong et al., 2019; Greybush et al., 2014) and therefore PEF represents a promising strategy towards enhancing their emission intensity and, in turn, expanding their application prospects (Dong et al., 2019; Greybush et al., 2014).

We note that the success of PEF-based applications relies on mastering various technical challenges, ranging from the theoretical understanding of coupling/interactions between plasmonic NPs and emitters for the design of appropriate PEF substrates, to their standardized and reproducible fabrication. Despite the diversity of available systems and self-assembly strategies, many of them result in a similar degree of structural control over the placement of AuNPs on the substrate. In order to emphasize this feature, we have organized the discussion according to strategies resulting in similar degrees of structural control over the placement of AuNPs, and their corresponding PEF effect. In addition, we propose different steps and directions for AuNP self-assembly, toward future applications.

2. General considerations on self-assembly of nanoparticles on a substrate

As mentioned in the previous section, NPs - often viewed as *'artificial atoms'*- serve as an attractive building block for the bottom-up self-assembly of macroscale materials. This comparison between NPs and atoms stems from the fact that the interactions between NPs can be viewed as *'bonds'*, discrete clusters as colloidal *'molecules'* and extended superlattices as *'crystals'*, which can be generated by controlling nanoscale bonding (Ashoori, 1996; Smith & Nie, 2010; Steigerwald & Brus, 1990). Appropriate surface engineering, size, and composition variation in nanomaterials provide suitable handles to tune interparticle interactions and lead to creation of self-assembled materials. Although most NPs are typically produced as colloidal dispersions in appropriate solvents, most devices/applications of interest around us require substrates that can be touched, controlled, or simply, interacted with. A key task then is to find ways of arranging NPs onto the substrates of interest. Furthermore, use of NPs as building blocks for self-assembly at interfaces allows for establishing control over the surface morphologies, through features that depend on the type of NPs used.

Having seen the possibility of using NPs as building blocks for self-assembly at interfaces, a relevant question is how to control the processes governing the deposition of NPs on substrates. The quality and outcome of the self-assembled structure requires control over the thermodynamic and kinetic aspects of the assembly process. Thermodynamics govern the interaction forces between building blocks, whereas kinetics control the speed of assembly. In other words, thermodynamics determine the energetically favored morphologies of the final assembled state, kinetics determine the extent to which the building blocks reach the energetically favored state. In general, the formation of high quality self-assembled structures requires weak reversible interactions, which would allow for *annealing* or *correcting* the defects produced (Whitesides & Boncheva, 2002). As a suitable model, crystallization involves slow and controlled interactions between the components, for high quality crystals to be formed. Since a random placement of NPs onto an interface requires minimal control, several strategies have been developed resulting in a random deposition of NPs. Although such methodologies may sound trivial, each protocol has its own set of challenges. One of the biggest hurdles is the notorious *coffee ring effect*: when a dispersion of NPs is evaporated on a substrate, it gives rise to ring-like deposits due to the migration of particles to the liquid-air contact line (Deegan et al., 1997). To overcome this effect, the substrate can be engineered to enhance a chemical binding of seeds, which can be subsequently grown or modified on the substrate. Alternatively, one can use more sophisticated techniques such as spin coating, dip coating, etc., for the deposition of randomly distributed NPs over the substrate of choice. Although these strategies are appealing due to their inherent simplicity and adaptability, the limited control over the NPs distribution is a critical challenge that limits their applications.

One of the key features dictating the interest of a self-assembly protocol is the control it provides over quality, crystallinity, and reproducibility of the desired outcome. To this effect, researchers have developed techniques to crystallize NPs into 2D or 3D ordered constructs. One such method is self-assembly at liquid interfaces, which provides a reliable and versatile way to produce highly ordered nanoparticle arrays. The morphology of drop-deposited nanoparticle films is controlled by both evaporation kinetics and interactions of particles with

the liquid–air interface (Min et al., 2008). Using this protocol, researchers have produced and characterized a rich variety of NP superlattices, most of which are isostructural with known atomic compounds (Shevchenko et al., 2006). Additionally, several discovered structures do not have analogues in the atomic world (Boneschanscher et al., 2013). Other techniques involve selective etching of NPs, thereby realizing the formation of non-close-packed superlattices (Figure 2a) (Udayabhaskararao et al., 2017). Examples of assembly of NPs into 3D crystals (assembly in bulk solution) can also be found in the literature (Auyeung et al., 2014; Jones et al., 2015; Laramy et al., 2019; Samanta et al., 2022). Chief among them is the use of DNA as a bonding element, leading to a rich variety of static, as well as dynamic or '*transmutable'* (Y. Kim et al., 2016; Macfarlane et al., 2013) 3D NP crystals. In addition to their photonic (D. J. Park et al., 2015), and catalytic functions (Brodin et al., 2015), assembled 3D NP crystals can serve as building blocks for the formation of macroscale materials as well. In this direction, Macfarlane and co-workers prepared 3D NP crystals glued together with H-Bonding interactions (Figure 2b), which could be *sintered* into bulk material. This strategy provides an excellent control over the crystal domains of the bulk material (Figure 2c,d), an attractive handle for photonic and mechanical applications (Santos et al., 2021).

In addition to delivering the material of interest onto desired places of a substrate, the orientations and contacts between the NP components, as well as between the assemblies and the substrate, should also be controlled. To meet the technological demands, researchers have developed hybrid techniques, thereby marrying the important aspects of two dissimilar methods. For instance, one can precisely control the location and orientation of NPs using approaches like capillarity, (micro)fluidics, or templated assembly, while retaining the simplicity and speed characteristic of a self-assembly process. For instance, Jacobs and co-workers demonstrated the implementation of an automated reel-to-reel fluidic self-assembly platform, which could assemble and electrically connect semiconductor chips with an assembly yield of 99.8%. This strategy could be scaled to any desired throughput, while outperforming the speed of chip placements using pick and place machines (S. C. Park et al., 2014). Additionally, capillary assembly techniques have been developed to achieve selective delivery of NPs into suitable target sites on a substrate, thereby achieving exceptional control over the final NP orientation (Figure 2e) (Cui et al., 2004; Ni et al., 2018). This strategy, therefore, allows for the precise definition of arbitrary topographic features distributed over large surfaces (Figure 2e) (Flauraud et al., 2017).

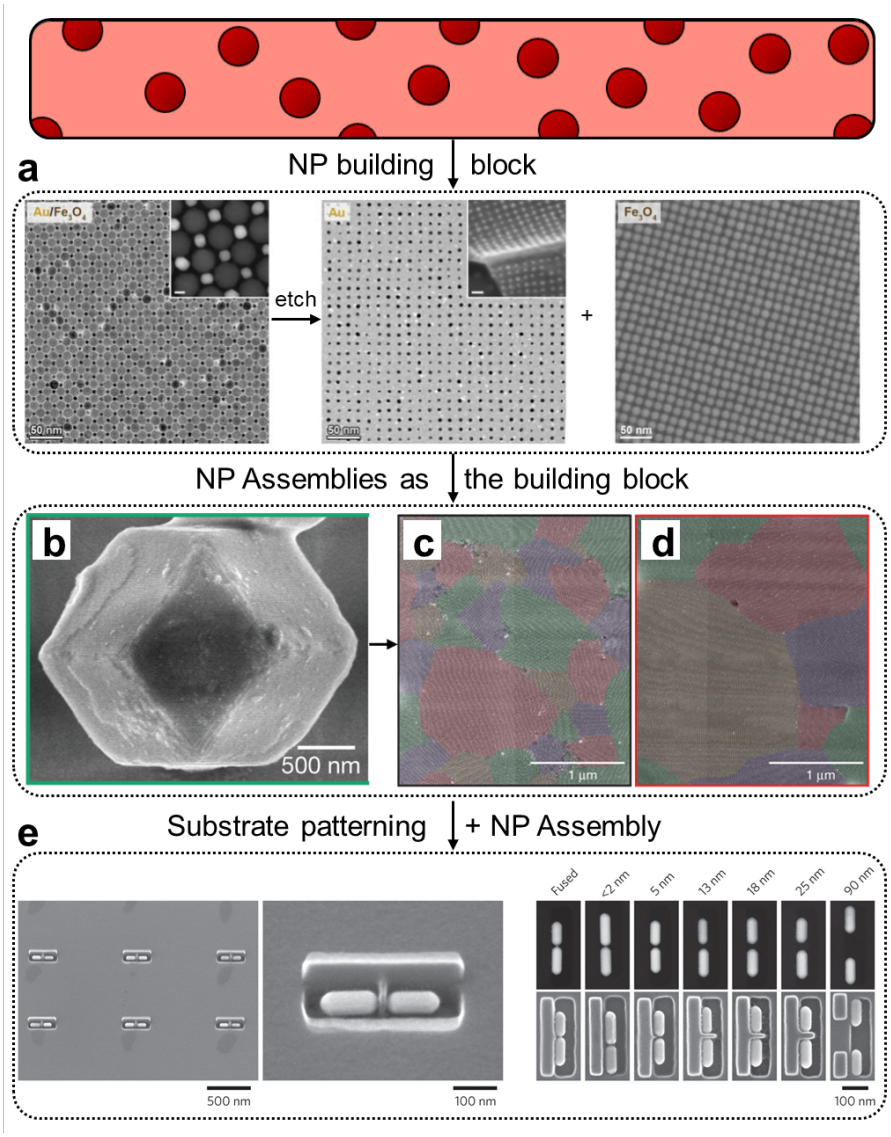

Figure 2. NPs into self-assembled materials. a) TEM images showing the transformation of a binary NP superlattice composed of gold (Au) and iron oxide (Fe_3O_4) NPs into non-close packed superlattices by selectively removing/ etching one of the two NP components. Inset scale bars are 5 nm (Udayabhaskararao et al., 2017). **b)** SEM image showing the surface morphology of a NP supercrystal stabilized by H-bonding interactions. Upon sintering into a macroscopic material an exceptional control can be gained over the grain size of the crystallites (**c, d**). Each crystalline grain is colored differently (Santos et al., 2021). **e)** SEM images showing the formation of Au nanorod (NR) dimers assembled using pre-defined cavities on a substrate. The SEM images on the right show the deterministic variation of interparticle distance between NR dimers (Flauraud et al., 2017).

It should be noted that, the remarkable progress made in the assembly of NPs on substrates is of significance for PEF studies. The self-assembly of metal NPs on planar substrates leads to stronger electric field enhancement, either at the metal surface or in the metal-metal nanogap areas, forming hot spots (Baumberg et al., 2019; Dong et al., 2015; Joyce et al., 2020; Semeniak et al., 2022) In the following section, we discuss self-assembly strategies that result in different degrees of structural control over the location of AuNPs on a substrate, and its associated PEF effect.

3. Plasmon enhanced fluorescence by Au nanoparticles on planar substrates

3.1 Strategies with limited structural control

3.1.1 Solution phase growth of AuNPs from a substrate

In this method, AuNPs are grown directly on the surface of (usually) planar substrates. In most cases, seeds are first implanted on the substrate, to then induce seeded growth, similar to the methods in solution. The resulting plasmonic Au nanoisland films are arguably among the most widely reported structures. The synthesis starts by immersing a glass slide into a solution of gold chloride ($HAuCl_4$), followed by addition of ammonium hydroxide (NH_4OH), washing, and a final immersion in sodium borohydride ($NaBH_4$) to complete the seeding step. Next, the seeded glass substrates are immersed into a 1:1 aqueous solution of $HAuCl_4$ and hydroxylamine (NH_2OH) as a weak reducing agent, followed by incubation under shaking to complete the growth step (Tabakman, Chen, et al., 2011; Tabakman, Lau, et al., 2011). This strategy results in elongated and tortuous Au nanostructures, with a shape similar to islands attached to the glass (Figure 3a) and broad plasmon resonances in the near-infrared region.

The name Au nanoisland film, also referred to as pGold slides (B. Liu et al., 2016), was initially proposed by Dai's group (Tabakman, Chen, et al., 2011; Tabakman, Lau, et al., 2011), and has been widely employed as a microarray PEF substrate in immunoassays to detect clinically-relevant target analytes (Semeniak et al., 2022). These include carcinoembryonic antigen (Tabakman, Lau, et al., 2011), cytokines (B. Zhang et al., 2012), antibodies against systemic lupus erythematosus (B. Zhang et al., 2013), autoantibodies for type I diabetes (B. Zhang et al., 2014), lung cancer biomarkers (B. Liu et al., 2016), autoantibodies for Toxoplasma gondii (X. Li et al., 2016), autoantibodies markers of hypertension (X. Li et al., 2017), autoantibodies against T. gondii, cytomegalovirus, and Rubella (X. Li et al., 2019), myocardial infarction biomarkers (Xu et al., 2020). Briefly, the capture antibody or antigen is attached to the Au nanoisland film, where it will bind the target analytes, followed by the binding of a second detection antibody labelled with fluorophores, such as Cy3, Cy5, IRDye680 and IRDye800 dyes (Figure 3b). The Au nanoisland film, composed of closely packed AuNPs separated by nanoscale gaps, generates an enhancement of the fluorescence emitted by these dyes. The highest reported fluorescence enhancement values were ∼50-fold (B. Liu et al., 2016; B. Zhang et al., 2014), ∼100-fold (X. Li et al., 2017; Tabakman, Lau, et al., 2011; B. Zhang et al., 2012, 2013, 2014) and ∼150-fold (Xu et al., 2020), compared to glass substrates (Figure 3c). The use of pGold has also been described in cellular imaging of Hela cells, by enhancing the immunostaining signals (Koh et al., 2016).

The Au nanoisland film strategy usually results in uncontrolled deposition of polydisperse AuNPs with varying shapes on the substrate (Figure 3a), and inhomogeneous dye distributions, so that only those located at non-quenching distances from the gold surface or in the nanogap would have an enhancement of the fluorescence intensity. Despite these limitations, this strategy presents the advantage of being a relatively simple synthesis protocol, and therefore, it has been widely reported (Table 1) in different PEF immunoassay studies (Semeniak et al., 2022), with improved sensitivity and reproducibility (Xu et al., 2020). To date, pGold slides are among the few PEF-based biosensors that have moved towards commercialization (Nirmidas Biotech, n.d.).

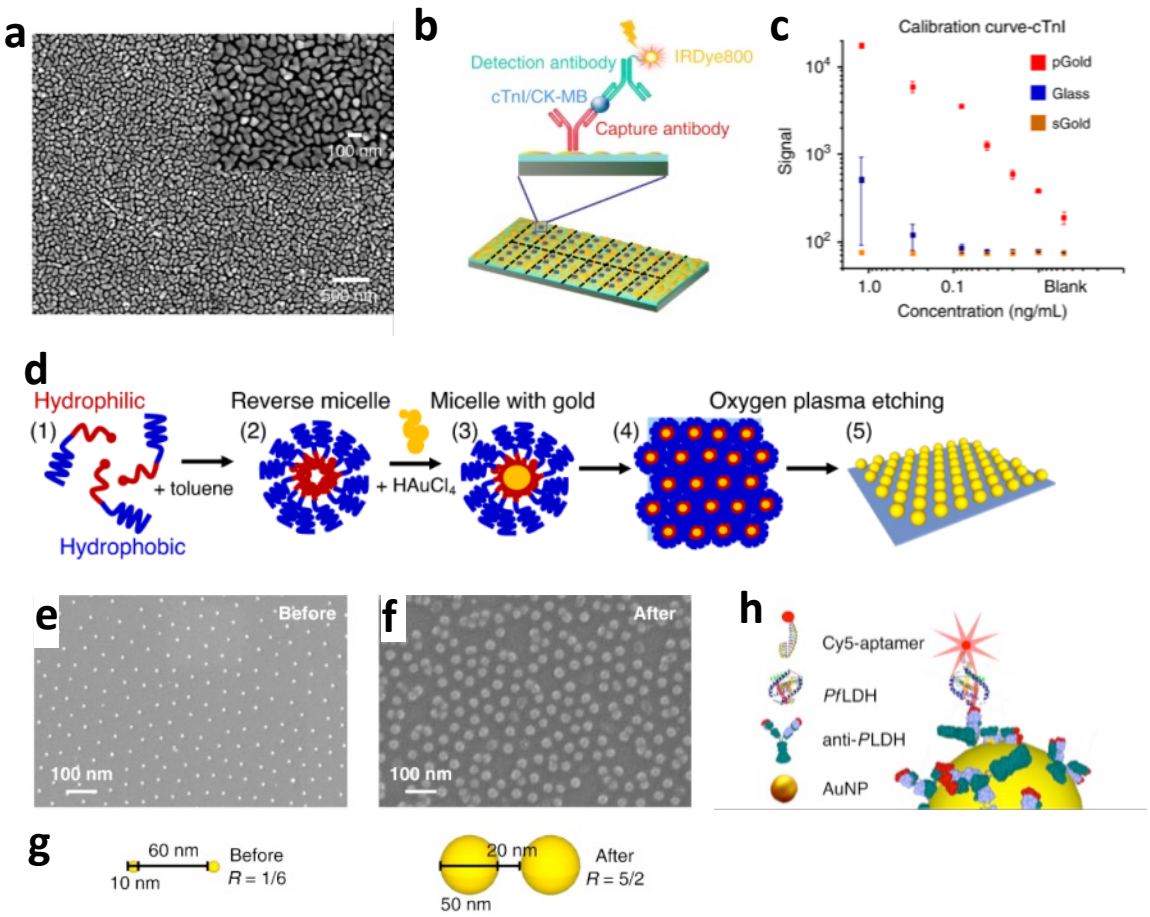

Figure 3. Solution phase growth of AuNPs directly on substrates. a) Scanning electron microscopy (SEM) image of a solution phase grown plasmonic Au nanoisland film pGold. **b)** Schematic illustration of a sandwich immunoassay for detecting myocardial infarction biomarkers (cTnI/CK-MB) on a pGold chip. **c)** Calibration curves comparing the fluorescence signal and detection limits for cTnI on pGold (red), glass (blue), and sputtered gold (sGold) (yellow) chips (Xu et al., 2020). **d)** Schematic of the solution phase growth of AuNPs on glass slides assisted by block copolymer micelle nanolithography (BCMN). **e)** SEM images showing the distribution of AuNPs after dip-coating and oxygen plasma for copolymer etching, before solution phase growth; and **f)** after the growth process. **g)** Schematic showing the interparticle distance in both cases. **h)** Immunoassay Ab-PfLDH-aptamer sandwich scheme. The fluorophore is placed at approximately 10 nm from the Au surface, maximizing fluorescence enhancement (Minopoli et al., 2022).

A more recent work utilized the well-known technique of block copolymer micelle nanolithography (BCMN)(Sánchez-Iglesias et al., 2010; Spatz et al., 1999) for the deposition and subsequent growth of AuNPs, enabling improved regularity of shape, size and interparticle distance between AuNPs on glass slides (Minopoli et al., 2020, 2022). Diblock copolymer reverse micelles with a hydrophilic core and an outer hydrophobic shell, where loaded with $HAuCl_4$ and then adsorbed on a glass substrate by dip-coating. The copolymers were subsequently etched by oxygen plasma treatment, followed by incubation with $HAuCl_4$ to enable the growth of the adsorbed AuNP seeds (Figure 3d). This procedure gives rise to a close-packed honeycomb type arrangement, enabling a high degree of control over interparticle distance (Figure 3e,f,g). This assembly method was employed in an immunoassay for detecting the malaria biomarker Plasmodium falciparum lactate dehydrogenase (PfLDH).

The detection was further improved by controlling the immobilization of antibodies via the photochemical immobilization technique (PIT), so that the binding region is at ~5 nm from the surface. At the same time, a small labelled aptamer (few nanometers) was used, so that the Cy5 dye was placed at an optimal distance of ~10 nm from the gold surface (Figure 3h). This latter feature, together with a good control over interparticle nanogaps may explain the claimed high experimentally measured enhancement factor of 7×10^4 in this system (Minopoli et al., 2020). Another work used a similar assembly strategy, in this case obtaining a double-resonant plasmonic substrate with plasmon peaks at 675 nm for a hexagonal AuNP pattern and 524 nm for isolated AuNPs, to match the spectra of 5-FAM and Cy5 dyes (Minopoli et al., 2022).

3.1.2 Electrostatic adsorption of AuNPs onto substrates

In this case, colloidal AuNPs are first synthesized and subsequently fixed on top of flat substrates. A strong adsorption can be achieved by exploiting electrostatic interactions. Both AuNPs and the substrate surface can be modified with appropriate molecules (ligands) of opposite charge, on which the fluorophore can be attached following the layer-by-layer self-assembly method (Malikova et al., 2002; S. Zhao et al., 2019) For example, glass slides modified with a positive amino group are immersed in a solution containing negatively charged citrate-stabilized Au nanospheres, leading to their spontaneous adsorption by electrostatic interaction. The layer-by-layer approach can then be applied through repeated dip-coating steps with positively and negatively charged polyelectrolytes and intermediate washing steps (Figure 4a) (Chekini et al., 2015).

Importantly, the layer-by-layer assembly allows using polyelectrolyte multilayers as spacers between AuNPs and fluorophores, thereby minimizing quenching and maximizing fluorescence enhancement. One such optimization was carried out for citrate Au nanospheres adsorbed onto aminated glass, followed by deposition of a polyelectrolyte spacer layer and then the dyes CF620R and Nile blue A, resulting in enhancements of 99 and 17.6-fold, respectively (Chekini et al., 2015). Besides fluorophores, this technique has also been described for the assembly of luminescent NPs, such as InP/ZnSe/ZnSeS/ZnS core/multiple shell quantum dots (QDs) (Kulakovich et al., 2021) and CdSe/ZnS core/shell QDs; the best enhancement factor in this case was 5-fold for ≈11 nm separation distance (Kulakovich et al., 2002). Additionally, Au nanorods were co-assembled with lanthanide-doped UCNPs, resulting in a highest fluorescence enhancement of 22.6-fold for 8 nm distance (Figure 4b,c,d,e) (Feng, You, et al., 2015). In a related study it was found that NaYF4:Yb,Er UCNPs could achieve 10.6-fold enhancement (Feng, Lin, et al., 2015).

Regarding applications, most of the strategies described in the literature (see Table 1) are related to immunoassays, with an architecture similar to that described in Figure 3b, where AuNPs are fixed onto a microarray glass surface by electrostatic interactions, rather than grown directly on the surface. Immunoassays with PEF substrates obtained by electrostatic interactions include Au nanorods or nano-crosses for the detection of hepatotoxins microcystin-LR (Y. Li et al., 2014), Au nanospheres to detect plasmodium falciparum lactate dehydrogenase (Minopoli et al., 2021), as well as a DNA biosensor (J. Wang & Jia, 2018). In a different architecture, positively charged Au core/Ag shell cubes and two sizes of Au nanorods were absorbed onto a negatively charged, flexible polydimethylsiloxane (PDMS) elastomeric film, with a polyelectrolyte spacer. This patch can be placed on top of standard fluorescence-

based microarrays or microtiter plates, thereby enabling emission enhancement of the dyes (Figure 4f,g). This plasmonic patch was tested in immunoassays for the detection of biomarkers such as kidney injury molecule-1 (KIM1) and neutrophil gelatinase-associated lipocalin (NGAL), showing a 100-fold enhancement (Luan et al., 2018).

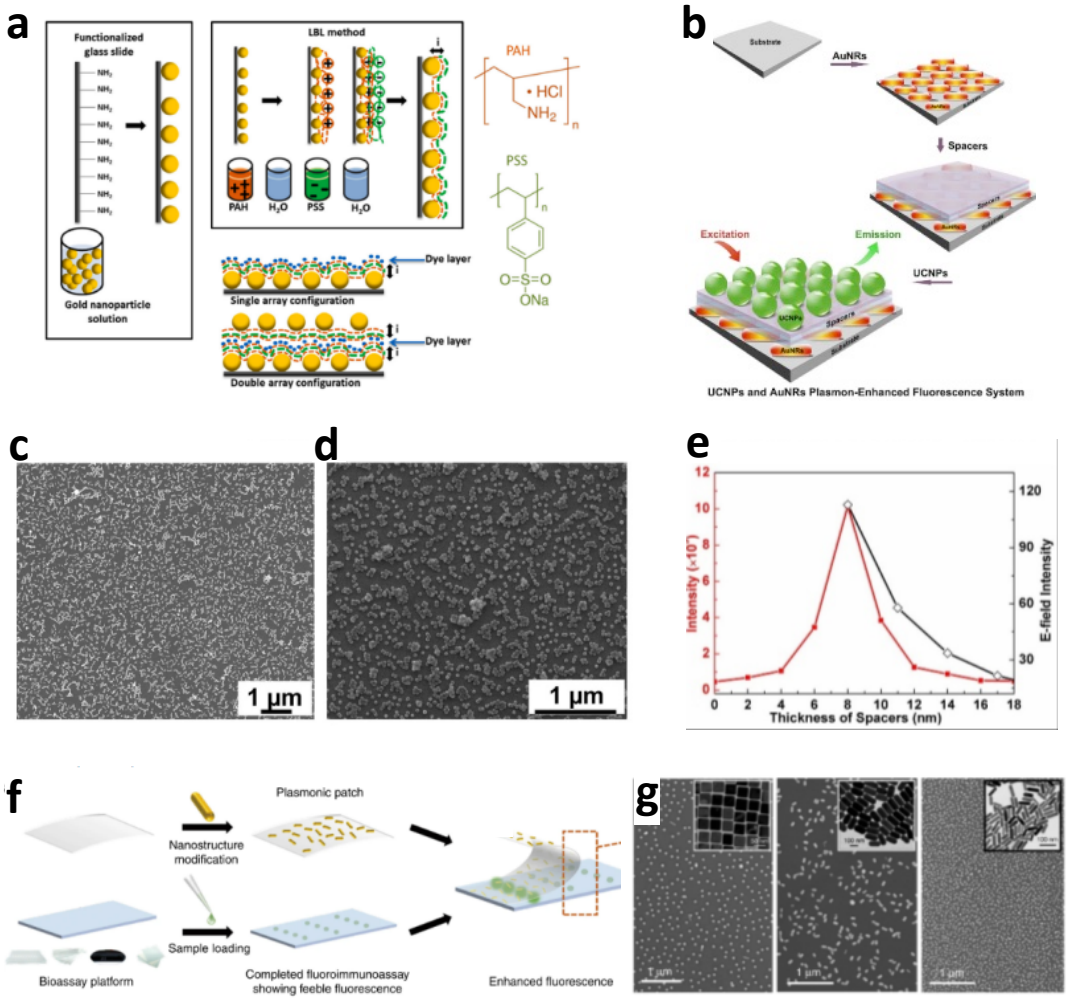

Figure 4. Adsorption of AuNPs onto substrates by electrostatic interactions. a) Schematic diagram of the adsorption of negatively charged citrate-coated AuNPs on positively charged amino functionalized glass slides, followed by layer-by-layer deposition of positive PHA and negative PSS polyelectrolytes, to form a spacer layer for the dye (Chekini et al., 2015). **b)** Schematic view of the self-assembly of Au nanorods on a silicon substrate, with a polyelectrolyte spacer and lanthanide-doped upconverting nanoparticles (UCNPs). **c)** Scanning electron microscopy images of Au nanorods and **d)** UCNPs, on the polyelectrolyte-coated substrate. **e)** Correlation of fluorescence intensity (red line) and electric field intensity (black line) with spacer thickness (Feng, You, et al., 2015). **f)** Schematic view of the fabrication of a flexible polydimethylsiloxane (PDMS) plasmonic patch with electrostatically adsorbed AuNPs and application of standard fluoroimmunoassays. **g)** SEM images of Au core/Ag shell cubes and two sizes of Au nanorods absorbed onto the PDMS plasmonic patch (Luan et al., 2018).

Overall, adsorption of AuNPs onto flat surfaces by electrostatic interactions is a relatively simple and widely studied method (Table 1). However, the main drawback is the poor control over the distribution of AuNPs, which assemble randomly on the substrate (Figure 4c,d,g).

3.1.3 Drop-cast, thiol-Au binding, spin coating, and DNA origami methods

Drop-casting is arguably one of the simplest assembly techniques, in which a drop of AuNP dispersion is placed on top of a substrate and dried. Although the AuNP distribution can hardly be controlled and is affected by the "coffee ring effect" with accumulation of NPs at the edges, these issues can be mitigated (S. Lee et al., 2022) by controlled evaporation conditions to obtain ordered structures (García-Lojo et al., 2019), as discussed in section 3.2.2. The drop-casting technique has been reported for the deposition of hybrid core/shell nanoparticles comprising an Au nanorod core with a SiO_2 shell spacer surrounded by CaF_2:Yb^{3+},Er^{3+} UCNPs. A SiO_2 shell thickness of ~20 nm maximized luminescence enhancement up to 6.7 for red emission (600-700 nm)(He et al., 2017). In another work, a mixture of Au nanorods and fluorescent nanodiamonds were drop-casted and the enhancement properties of selected pairs studied (J. Zhao et al., 2018), revealing that both Au nanorods and fluorescent nanodiamonds mutually enhance their light emission; for Au nanorods this was verified by an increase in the anti-Stokes emission (J. Zhao et al., 2018).

Thiol–Au binding is another useful method for the attachment of AuNPs onto substrates functionalized with thiol groups. For example, both small (~50 nm) and large (215 nm) Au nanostars were bound to thiol-modified glass slides by simple immersion in the corresponding colloid (Figure 5a). The approach was used for imaging Hela cells cultured on top of the nanostars and immunostained with AlexaFluor680 antibodies. Compared to plain glass, the Au nanostars yielded 9 and 19 times fluorescence enhancement factors for small and large nanostars, respectively (Theodorou et al., 2019).

Spin-coating is a relatively common method for applying thin films, involving the spinning of flat substrates at high velocity, after deposition of the material in solution (Scriven, 1988). The centripetal force and surface tension of the liquid allow creating thin films with uniform thickness, from few nanometers to few microns. Spin coating is a standard technique used in a wide range of industry sectors (Barad et al., 2021).

Au nanospheres and nanorods were spin-coated onto larger area flat glass substrates (Ullrich et al., 2013). The synthesized AuNPs were functionalized by thiol-terminated polystyrene with different molecular weights, spin-coated, and the polymer shell was then removed by plasma etching (Figure 5b1). Spin coating, together with the dense shell of polystyrene surrounding the AuNPs, led to the formation of ordered patterns of Au nanospheres (Figure 5b2) and NRs (Figure 5b3), where the particle-to-particle distance depended on the length of the polystyrene shell (Ullrich et al., 2013). It should be noted however, that highly organized monolayers of AuNPs functionalized with hydrophobic or hydrophilic ligands can also be obtained without the need for spin-coating, namely by interfacial self-assembly (section 3.2.1) or controlled evaporation self-assembly (section 3.2.2), as discussed further below.

Spin-coating has been used widely as a technique to self-assemble AuNPs in PEF studies (Table 1). Namely, Au nanorods were spin-coated and covered layer-by-layer by a polymer spacer to measure Cy3.5 single molecules and mCherry fluorescent proteins in solution, one at a time as they adsorb onto the immobilized Au nanorods (Donehue et al., 2014; Fu et al., 2015). A similar approach was also used to study the enhancement of single CdSe/ZnS QDs with two-photon excitation, using bare Au nanorods (W. Zhang et al., 2018). Another study combined

drop-casting of Au nanostars followed by spin-coating of NaGd(Y)F4 UCNPs (Martínez et al., 2018).

The group of Ramamurthy reported several works using a Surface Plasmon-Coupled Emission (SPCE) sensing platform (Figure 5c1). Spin-coating was used to assemble diverse types of AuNPs and fluorescence emitters, to obtain various nanointerface designs onto a silver film substrate in the SPCE platform (Bhaskar et al., 2021, 2022; Bhaskar, Kowshik, et al., 2020; Bhaskar, Patra, et al., 2020). One of the highest reported enhancement factors, in excess of 1300 (Figure 5c3), was achieved in a SPCE sensor, to detect mefenamic acid using heterometallic AgAu nanocubes (Figure 5c2) (Bhaskar et al., 2022).

Overall, the advantage of spin coating is that only a relatively small volume of concentrated AuNP suspension is needed to cover a larger area substrate.

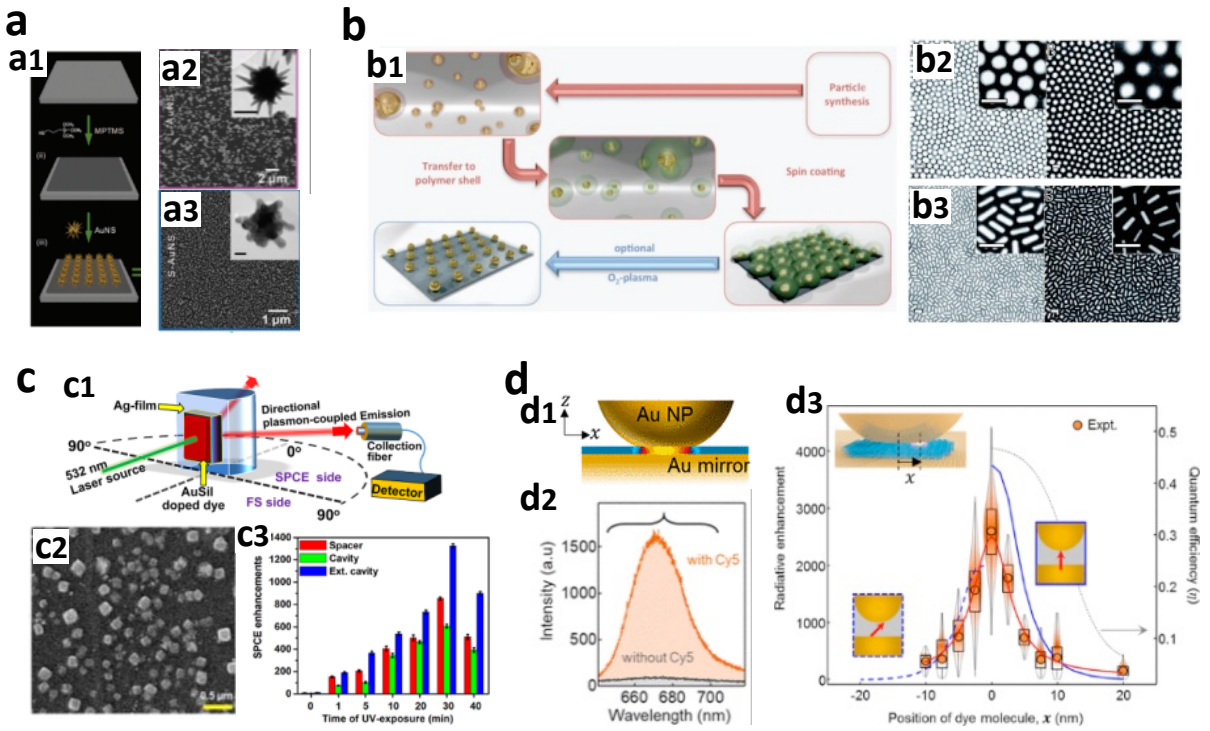

Figure 5. a) Thiol–Au binding of AuNPs. a1) Schematic of Au nanostars bound to thiol-modified glass slides. Corresponding **a2)** SEM images of adsorbed small (~50 nm) and **a3)** large (215 nm) Au nanostars (insert: TEM of individual nanostars) (Theodorou et al., 2019). **b) Spin-coating of AuNPs. b1)** Schematic showing AuNPs functionalized with a dense polystyrene shell, followed by spin-coating onto a substrate and oxygen plasma etching of the polystyrene shell. **b2)** SEM images of Au nanospheres and **b3)** Au nanorods with shorter (left) and larger (right) polystyrene chains (Ullrich et al., 2013). **c) Surface plasmon-coupled emission (SPCE) sensor with spin-coasted AuNPs. c1)** Schematic of the SPCE sensing platform. (Bhaskar, Kowshik, et al., 2020). **c2)** SEM image of heterometallic AgAu nanocubes. **c3)** Fluorescent enhancement values obtained for different nanointerface designs (Bhaskar et al., 2022). **d) Nanoparticle-on-mirror** (NPoM) **nanocavities**. **d1)** Schematic showing the high optical field confinement in the gap (yellow) and **d2)** fluorescence emission with and without the Cy5 dye incorporated into the nanocavity. **d3)** Purcell enhancement results relative to the position of Cy5 from the center of the gap, experimental emission (orange points) and theoretically calculated emission for vertical (90°) dipole (solid blue) and tilted (45°) dipole (dashed blue). Calculated quantum efficiency for vertical dipole (dashed gray line) (Chikkaraddy et al., 2018).

In most cases, fluorescence emitters placed at a very close distance (less than 5 nm) to isolated AuNPs are affected by quenching of the emission. This is not necessarily the case for metal-metal plasmonic nanocavities, such as **nanoparticle-on-mirror** (NPoM) **nanocavities,** where high optical field confinement in the gap (at distances less than 5nm) (Figure 5d) suppresses emitter quenching into non-radiative channels and highly enhances the emission (Baumberg et al., 2019). This makes NPoM interesting for PEF, in which colloidal metal NPs are usually assembled on top of metal substrate thin films. Control of the metal-metal distance and accurate placement of the emitters into the nanocavity are critical. Different approaches have been described in the literature to obtain NPoMs with AuNPs, including drop-casting using a molecular spacer (Chikkaraddy et al., 2016), attachment with DNA origami constructs (Chikkaraddy et al., 2018; Kongsuwan et al., 2018), and adsorption by electrostatic interactions (Ciracì et al., 2012; Mock et al., 2008; Xie et al., 2021) as described in section 3.1.2 above. For example, colloidal Au nanoshells were adsorbed onto an Au film by electrostatic interactions and used together with Rhodamine B to fabricate an SPCE based immunosensor for detection of human IgG, reaching enhancements of 30-fold and 110-fold, compared to normal SPCE and free-space emission, respectively (Xie et al., 2021).

The group of Baumberg reported several studies with NPoM nanocavities. These include, Au nanospheres drop-casted on an Au thin film separated by a 0.9-nm molecular spacer composed of methylene-blue dye encapsulated in cucurbit[7]uril. The latter formed a monolayer on the Au film and allowed the dye to be perfectly oriented into the molecular structure, thereby preventing aggregation; this work claimed simulated Purcell factor enhancements of 3.5×10^6 (Baumberg et al., 2019). Another strategy comprised the use of a **DNA origami construct** modified with thiol groups, to attach first onto the gold substrate film, followed by addition of colloidal Au nanospheres. By generating a nanocavity with less than 5 nm gap between two plasmonic components with a chemically precisely placed single molecule of Cy5 dye (Figure 5d) (Chikkaraddy et al., 2018; Kongsuwan et al., 2018), the fluorescence emission with the Cy5 dye in the nanocavity revealed a strongly enhanced intensity (Figure 5d2) and a Purcell factor enhancement up to ≥ 4000 (Figure 5d3). The signal decreased when the dye moved a few nm away from the center of the gap, thus confirming the importance of a precise positioning of the emitter in the nanocavity, to match the nanovolume of highest electromagnetic field enhancement (Figure 5d1) (Chikkaraddy et al., 2018).

NPoM studies from other groups used fluorescent emitters molecules as spacers to control the gap distance, such as Au nanospheres coated with a polypyrrole emitter of varying thickness, drop-casted on an Au film. The emission signal achieved an enhancement factor of up to ~7000 for a 7 nm polypyrrole shell thickness (Y. Wang & Ding, 2019). Other NPoM works used luminescent NPs (Goßler et al., 2019; Sugimoto et al., 2018), such as silicon QDs (Si QDs) dispersed in methanol and drop-cast on an Au film forming monolayers, followed by addition of Au nanorods on top. In this case, the gap corresponds to the Si QDs diameter of 3 nm, sandwiched between the Au nanorods and the Au film, resulting in an enhancement factor greater than 900 (Sugimoto et al., 2018).

Overall, in NPoM nanocavities the distances between the metal and the fluorescence emitter can be reduced to around or even less than 5 nm without quenching, while these nanocavities

often provide far greater enhancement of the fluorescence emission, compared to isolated AuNPs or AuNPs on glass substrates (Table 1).

3.2 Strategies with high structural control

3.2.1 Interfacial self-assembly

Suitable functionalization of NP surfaces can be exploited to trap them at the interface between two immiscible phases, where they will form an organized layer due to interfacial phenomena (Figure 6a), such as electrostatic interactions, capillarity, and van der Waals forces. The Langmuir–Blodgett (LB) method is a classic example of this technique, which utilizes the liquid-air interface to self-assemble NPs into ordered monolayers, subsequently compressed by using a so-called LB trough, and then transferred onto substrates, producing extended closely-packed monolayers (Vogel et al., 2015).

Interfacial self-assembly has been used to prepare plasmonic substrates composed of different AuNP types and then applied in proof-of-concept Fluorescence Resonance Energy Transfer (FRET)-based DNA microarrays or for FRET imaging of live cells (Hou et al., 2020). Synthesized Au@Ag nanocubes, Au@Ag nanorods, and Au nanorods, with different plasmon resonances (Figure 6b) to match the excitation and emission wavelengths of the fluorophores (BDP-FL, Cy5, and IR-800CW), were modified with polydopamine (PDA), which also acted as a spacer, and mixed with chloroform. AuNPs formed a film at the water/chloroform interface, water was then carefully removed and a glass slide dipped into the chloroform and slowly lifted (Figure 6a), resulting in coating of the slide with a monolayer of AuNPs (Figure 6c). The resulting plasmonic substrates were tested on a total internal reflection fluorescence (TIRF) microscope for the imaging of live MDA-MB-468 cells, using a Cy3/Cy5 FRET probe to label the cell membrane (Figure 6d). Fluorescence images using a plasmonic substrate with Au@Ag nanorods, best matching the Cy5 dye optical spectra, showed a significant enhancement of the fluorescence signal compared to bare glass (Figure 6e,f) (Hou et al., 2020). This work demonstrated the versatility of self-assembling AuNPs with tailored plasmon resonances to obtain plasmonic substrates matching the optical properties of different fluorophore emitters and maximize enhancement.

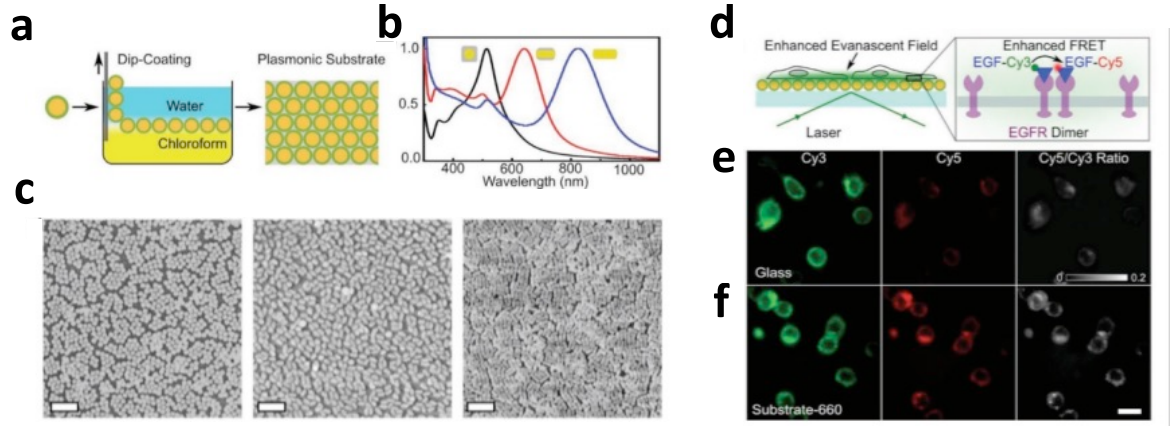

Figure 6. Interfacial assembly of AuNPs. a) Schematic of the fabrication of plasmonic substrates by interfacial assembly, AuNPs organized into monolayers at the water/chloroform interface are transferred to a glass substrate. **b)** Extinction spectra of substrates obtained by assembly of Au@Ag nanocubes, Au@Ag nanorods, and Au nanorods, respectively. **c)** SEM of the assembled plasmonic substrates on glass slides (scale bars: 400 nm). **d)** Schematic of total internal reflection fluorescence (TIRF) microscopy using interfacially assembled plasmonic substrates with enhanced fluorescence resonance energy transfer (FRET) imaging. **e)** Fluorescence images of MDA-MB-468 cells on glass and **f)** on a plasmonic substrate (scale bar: 20 μm) (Hou et al., 2020)**.**

3.2.2 Controlled evaporation self-assembly

In this method, a droplet of a NP colloid is evaporated on top of the substrate under controlled conditions of temperature and humidity (Figure 7a1). Due to solvent evaporation, as the NPs concentration increases to a critical volume, capillary forces pull the NPs closer together driving the self-assembly. Controlled evaporation self-assembly has been applied for example to fabricate ordered 2D or 3D supercrystals (García-Lojo et al., 2019; Z. Li et al., 2022), eventually used in PEF studies, for example to improve the luminescence efficiency of UCNPs (Figure 7a3) (Yin et al., 2016). In this study, a dispersion of CTAB-stabilized AuNRs was left to evaporate over 24h under controlled temperature of (21 °C) and humidity (~70%) (Figure 7a1). As a result, the Au nanorods (Figure 7a2) self-assembled into vertically aligned monolayer supercrystals on the glass substrate (Figure 7a4), is possible to see the contrast compared to random aggregated Au nanorods (Figure 7a5). Then a MoO_3 spacer was used to optimize the distance between the Au surface and $NaYF_4$:Yb^{3+},Er^{3+} UCNPs. The spacer thickness of ∼8 nm produced the highest enhancement factor, with a 35-fold value (Yin et al., 2016)**.**

Additionally, the controlled evaporation approach was used to obtain ordered AuNR monolayer array chips and demonstrate DNA probe detection (Mei & Tang, 2017). In this case, the Au nanorods were functionalized with a thiol-modified hairpin ssDNA carrying the Quasar670 dye on the 5' position, which is quenched due to proximity to the Au surface. Upon hybridization with the complementary ssDNA, the hairpin loop was opened, thereby extending the dye molecule ∼16 nm away from the gold surface, in turn resulting in a maximum of enhanced fluorescence (Mei & Tang, 2017).

Controlled evaporation thus allows to generate ordered AuNPs, but has the limitation of low precision on the location and dimensions of these assemblies on the substrate, most often being restricted to the location/size of the initial colloid drop.

3.2.3 Template-controlled self-assembly

This is a slightly more sophisticated approach, in which a two-dimensional, topographically pre-structured, patterned template is used to direct the assembly of AuNPs from solution, thereby providing a high degree of structural control and precise location of AuNP superlattices on the substrate (García-Lojo et al., 2019; Hamon & Liz-Marzán, 2015; Z. Li et al., 2022).

Different types of template-controlled assembly have been reported. For example, it is possible to use a PDMS mold with cavities, together with a high concentration of AuNPs (Figure 7b1); upon drying and careful removal of the PDMS mold highly organized supercrystal arrays are obtained, with features that can be as small as 200 nm (Hanske et al., 2019). This work also showed that the composition of the solvent may be crucial, as exemplified by the deposition of standing or laying Au nanorods when water or water/ethanol mixtures, respectively, were used (Figure 7b2,b3).

In the case of **capillary-assisted self-assembly**, the principle is based on a controlled de-wetting process. A dispersion of NPs forms a moving liquid evaporating meniscus interface, in which the NPs are concentrated and trapped by capillary forces into the topographical

cavities of a template (Figure 7c). The size and shape of the template cavities can be selected by lithography techniques in silicon substrates, thereby enabling the precise position of isolated NPs in a template substrate array (Ni et al., 2018).

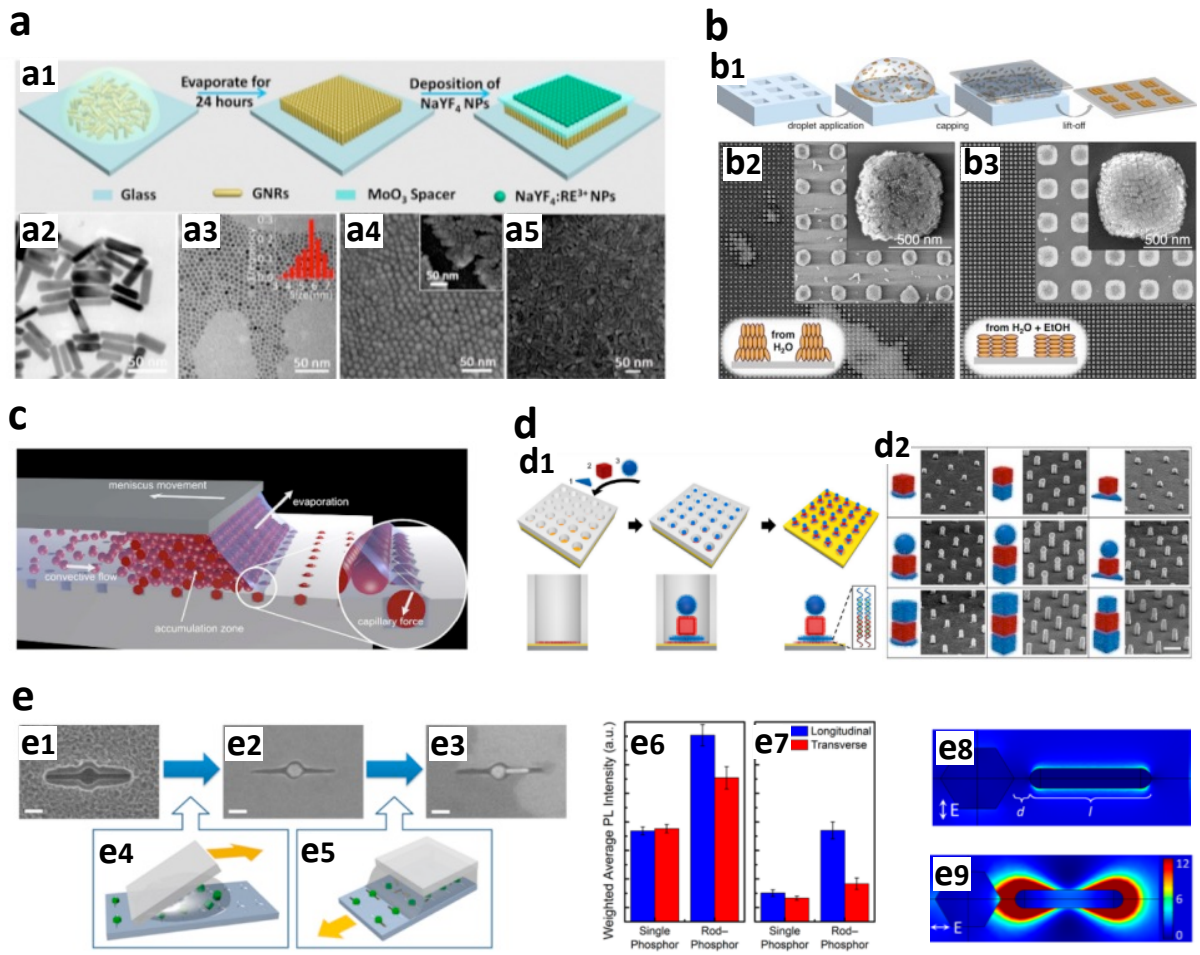

Figure 7. a) Controlled-evaporation self-assembly. a1) Schematic of the process: a drop of AuNR dispersion is evaporated under controlled conditions, originating a vertically aligned monolayer of Au nanorods, followed by the deposition of $NaYF_4:Yb^{3+},Er^{3+}$ upconversion nanoparticles (UCNP), separated by a MoO_3 spacer. **a2)** TEM images of Au nanorods and **a3)** UCNP. **a4)** SEM images of vertically aligned Au nanorods (insert, side view) and **a5)** random aggregates of Au nanorods (Yin et al., 2016). **b) Template-controlled self-assembly. b1)** Schematic depicting a drop of AuNP dispersion confined between the PDMS mold and the substrate; upon drying and PDMS lift-off organized supercrystals are obtained. **b2)** SEM images of standing AuNRs obtained when dispersed in water or **b3)** laying AuNR supercrystal arrays when dispersed in a water/ethanol mixture (Hanske et al., 2019). **c) Schematic of capillary-assisted self-assembly,** AuNPs are directed and trapped into template cavities by capillary forces (Ni et al., 2018). **d) DNA-assisted self-assembly. d1)** Schematic of polymer PMMA holes and sequential assembly of ssDNA-modified AuNPs with complementary sequences. **d2)** SEM images of two- and three-layer stacks of AuNP superlattices (scale bar: 300 nm) (Lin et al., 2018). **e) Templated self-assembly of heterodimers composed of UCNP and AuNR on a silicon substrate.** SEM images of **e1)** empty cavities, **e2)** single UCNP and **e3)** heterodimer UCNP/AuNR in SiO_2 template (Scale bars: 100 nm). **e4)** Schematic of UCNP assembly with "squeegee method" and **e5)** AuNRs positioned in the cavities by capillary-assisted assembly. **e6)** Inverse-variance weighted average photoluminescence (PL) intensity for a power density of 1.6 $x10^6$ W/cm^2 and **e7)** 1.6 $x10^5$ W/cm^2. **e8)** simulated transverse and **e9)** longitudinal excitation polarization field intensity enhancement maps. (Greybush et al., 2014).

Recent developments with **DNA-assisted self-assembly** have enabled the controlled formation of individual 3D arrays of stacked NPs (Lin et al., 2018). Here, an array of pores was fabricated in a PMMA-coated gold substrate by electron beam lithography, and its bottom was modified with DNA. By sequential immersion in a dispersion of AuNPs functionalized with DNA sequences complementary to the previous one (Figure 7d1), stacks of AuNPs are created (Figure 7d2).

Few studies can be found in the literature, where templated self-assembly of colloidal AuNPs is associated with PEF (Table 1). One example was provided by Murray and Kagan et al.(Greybush et al., 2014), who demonstrated plasmon-induced fluorescence enhancement of individual dimers comprising $NaYF_4$:Yb^{3+},Er^{3+} UCNPs and AuNRs placed by capillary-assisted self-assembly on a silicon template (Greybush et al., 2014). In this study, the template pattern was prepared by electron beam lithography (EBL), leading to cavities on the silicon substrate. The shape of the cavities was selected so that individual UCNPs were located at the center and the extended arms of the template could accommodate individual AuNRs (Figure 7e1). The UCNPs were assembled by a "squeegee method" (Figure 7e4) (Saboktakin et al., 2013), where a drop of UCNPs colloid in hexane was dragged across the surface with a piece of PDMS to assemble them into the template, followed by removal of PMMA and deposition of a thin 6 nm layer of SiO_2 by atomic layer deposition (Figure 7e2). This technique secured the UCNPs in place and provided a spacer to avoid quenching by AuNRs too close to UCNPs. The process was followed by capillary-assisted self-assembly of AuNRs, by depositing a drop of AuNR colloid between a fixed glass slide and the substrate, which was slowly moved on a translation stage (Figure 7e5). The meniscus moved along the template, thereby driving and trapping the AuNRs into the cavities by capillary forces (Figure 7e3).

This study claimed several-fold enhancement of the emission by AuNP/UCNP dimers compared to single UCNPs, as well as a dependence on the excitation laser polarization relative to the AuNR axis (Figure 7e6, e7). More precisely, a longitudinal polarization resulted in higher enhancement compared to the transverse polarization, in agreement with simulations showing that the field intensity is amplified at the AuNR tip where the UCNP is positioned (Figure 7e8, e9).

Overall, templated self-assembly provides a high level of control on the location of AuNPs on the substrate. As a limitation, one can mention that it is a more complex method, requires additional steps, optimization, and uses more advanced instrumentation, such as lithography techniques, to obtain isolated AuNPs arrays.

4. Conclusions and Future Directions

To conclude, one of the next key challenges in the field of bottom-up self-assembly involves the use of purposely synthesized AuNPs with the desired properties for crafting/assembling micro- or macroscale materials. We propose that self-assembly protocols not only will champion the assembly of high-quality structures, but will also deliver those assemblies of interest on the desired locations on a substrate, with a high degree of control.

In the present review, we have summarized different strategies and studies involving increasing structural control over AuNPs self-assembled on planar substrates, focusing on their PEF effect. The development of these structures is presented in terms of an increasing structural control over the final self-assembled state. We note however, that most of the existing studies exploiting self-assembly techniques give rise to random or rather limited control over the distribution of AuNPs on the substrate. Additional studies are needed, which involve plasmonic substrates with a higher degree of control over the placement of AuNPs. Moreover, most PEF studies have been carried out within the field of biosensing, where the plasmonic substrates are typically used as immunoassay platforms, whereas a minority of studies are targeting bioimaging applications. Incidentally, plasmonic substrates are also commonly used to drive emission enhancement from UCNPs, QDs, etc. Importantly, the highest fluorescence enhancement factors have been described for self-assembly strategies involving the formation of metal-metal nanogaps, such as NPoM geometries. In this construct, an accurate control over the metal-metal distance, as well as a precise placement of the emitter, are of paramount importance.

We envision increasing opportunities for AuNP self-assembly strategies that provide high structural control. For instance, one can exploit the localized electric field enhancements around the tips of Au nanorods or Au bipyramids, by assembling the emitters through templated or capillary assembly protocols. Alternatively, studies can be undertaken to prepare superlattices with plasmonic AuNPs and QDs. Recent progress in the preparation of non-close packed self-assemblies of plasmonic AuNPs has allowed the localization of emitters in environments with varying electric field intensities. Lastly, we note that the field of controlled, templated self-assembly has seen the realization of lattice plasmon resonances, through the organization of plasmonic NP arrays that enable far-field coupling of the scattered light, giving rise to plasmon resonances with bandwidths as narrow as a few nanometers (Scarabelli et al., 2021). A similar organization of perovskite NPs into photonic architectures has resulted in enhanced electric field intensities, producing amplified spontaneous emission under low laser fluences (Vila-Liarte et al., 2020). These studies could be extended to the field of PEF, where not only appropriately placed plasmonic AuNPs, but also structural factors like lattice spacing, photonic architectures, etc., can be used to modify and improve the optoelectronic response of the system.

Table 1 – Plasmon fluorescence enhancement studies of colloidal AuNPs on planar substrates. The type of spacer and distance normally refer to the spacer thickness, meaning the distance between the emitter and the gold surface, except when indicated otherwise # please see reference for details.

Self-assembly strategy	Application (Description)	NPs type (Substrate)	Enhancement factor (Emitter) [Spacer and distance]	Reference
Solution phase growth	Microarray immunoassay (carcinoembryonic antigen)	Au nanoislands film (glass)	~100-fold(IR800), ~15-fold (Cy5)	(Tabakman, Lau, et al., 2011)
	Microarray immunoassay (panel of 6 cytokines)	Au nanoislands film (glass)	~100-fold (IRDye 800)	(B. Zhang et al., 2012)
	Microarray immunoassay (antibodies against systemic lupus erythematosus)	Au nanoislands film (glass)	~100-fold (IRDye 800)	(B. Zhang et al., 2013)
	Microarray (autoantibodies for type I diabetes)	Au nanoislands film (glass)	~100 (IRDye800), ~50 (Cy5), ~30-fold (Cy3)	(B. Zhang et al., 2014)
	Microarray (Lung cancer biomarkers)	Au nanoislands film, pGOLD (glass)	~50-fold (IRDye800)	(B. Liu et al., 2016)
	Microarray (Autoantibodies for Toxoplasma gondii)	Au nanoislands film (glass)	N/A (Cy3, IRDye680, IRDye800)	(X. Li et al., 2016)
	Cellular imaging (Immunostaining of tubulin, HER2, EGFR)	Au nanoislands film, pGOLD (glass)	~2.7 (Cy3),~3.3(Cy5), ~18 (IRDye680), ~21-fold (IRDye800)	(Koh et al., 2016)
	Microarray (Autoantibodies markers of hypertension)	Au nanoislands film (glass)	~100-fold (IRDye800)	(X. Li et al., 2017)
	Microarray (Autoantibodies against T. gondii, cytomegalovirus, and Rubella)	Au nanoislands film, pGOLD (glass)	N/A(IRDye800, IRDye680)	(X. Li et al., 2019)
	Antibody microarray (myocardial infarction markers)	Au nanoislands film, pGOLD (glass)	~130-fold (IRDye800)	(Xu et al., 2020)
Solution phase growth, assisted by block copolymer micelles	Immunoassay (Plasmodium falciparum lactate dehydrogenase)	Hexagonally arranged Au NPs (glass)	70000 (Cy5) [antibody/ aptamer ~10nm]	(Minopoli et al., 2020)
	Immunoassay (Plasmodium falciparum lactate dehydrogenase)	Hexagonally arranged AuNPs, isolated AuNPs (glass)	160 (5-FAM), 4500 (Cy5) [antibody/ aptamer 5-10nm]	(Minopoli et al., 2022)
Electrostatic interactions	Basic Research (optimize spacer distance)	Au nanospheres (glass)	5-fold ((CdSe)ZnS QDs) [polyelectrolytes ~11 nm]	(Kulakovich et al., 2002)
	Immunosensor (hepatotoxins microcystin-LR)	Au nanorods or nano-crosses (glass)	2.3- to 35-fold (Cy5) [protein/antibodies 20.3 nm	(Y. Li et al., 2014)
	Basic Research (optimize spacer distance)	Au nanospheres (glass)	99-fold (CF620R), 17.6-fold(Nile blue A)	(Chekini et al., 2015)
	Basic Research (optimize spacer distance)	Au nanorods (silicon)	22.6-fold (Lanthanide-doped UCNPs) [polyelectrolytes 8 nm]	(Feng, You, et al., 2015)
	Basic Research (optimize spacer distance)	Au nanorods (silicon)	10.6-fold ($NaYF_4$:Yb,Er UCNPs) [polyelectrolytes 8 nm]	(Feng, Lin, et al., 2015)
	Microarray immunoassay (Kidney injury molecule 1, neutrophil gelatinase-associated lipocalin)	Au nanorods, Au core/Ag shell cubes (PDMS)	Up to 10.3-fold (LT680, 800CW)	(Luan et al., 2018)
	DNA biosensor (hybridization with labeled ssDNA)	Au NPs (porous silicon)	2-fold (Rhodamine red)	(J. Wang & Jia, 2018)
	Basic Research (optimizing enhancement)	Au and Ag nanospheres (glass)	1.8-fold (InP/ZnSe/ ZnSeS/ZnS QD)	(Kulakovich et al., 2021)
	Immunoassay (Plasmodium falciparum lactate dehydrogenase)	Au nanospheres (glass)	340-fold (5-FAM) [antibody/ aptamer, ~10nm]	(Minopoli et al., 2021)
	Basic Research and Immunosensor (human IgG) - SPCE sensor	Au nanoshells (gold film)	Up to 110 -fold (RhB) [#dye doped PVA film 30 nm]	(Xie et al., 2021)
Drop-casting	Basic Research (enhance emission from UCPL)	Au nanorod@SiO2 @CaF2:Yb3+,Er3+ hybrids (glass)	6.7 (CaF_2:Yb^{3+},Er^{3+} UCNP) [SiO_2 spacer ~20 nm]	(He et al., 2017)
	Basic Research (nanoparticle-on-mirror)	Au nanospheres (Au film)	Purcell factor 3.5×10^6 (methylene-blue), [# encapsulated in cucurbit[7]uril 0.9 nm]	(Chikkaraddy et al., 2016)

	Basic Research (thermoplasmonic enhancement)	Au nanostars (glass)	N/A ($NaGd(Y)F_4$ UCNP)	(Martínez et al., 2018)
	Basic Research (enhance emission from FNDs)	Au nanorods (glass)	(Fluorescent Nanodiamonds (FNDs))	(J. Zhao et al., 2018)
	Basic Research (nanoparticle-on-mirror)	Au nanorods (Au film)	>900-fold (silicon QDs) [# monolayer of QDs size 3 nm]	(Sugimoto et al., 2018)
	Basic Research (nanoparticle-on-mirror)	Au nanospheres and Ag cubes (Au film)	>1000 (AIS/ZnS QDs) [#polymer and surfactant spacer sub 10 nm]	(Goßler et al., 2019)
	Basic Research (nanoparticle-on-mirror)	Au nanospheres (Au film)	~7000 (pyrrole) [#polypyrrole shell of 7 nm]	(Y. Wang & Ding, 2019)
	Basic Research (enhance emission from QDs)	Au nanorods (glass)	7.2-fold (silicon QDs) [SiO_2 spacer ~5 nm]	(Pavelka et al., 2021)
Blade coating	Basic Research (enhance emission from UCPL)	AuNPs	(YF/YOF:Yb3+,Er3+ UCNPs)	(Ngo et al., 2022)
Thiol–Au binding	Bioimaging of Hela cells (folate receptor alpha (FRα) labelled antibody)	Au nanostars (glass)	Up to 19-fold (AF-680)	(Theodorou et al., 2019)
DNA origami assisted attachment	Basic Research (nanoparticle-on-mirror)	Au nanospheres (Au film)	Purcell factor ≥4000 (Cy5), [# integrated in DNA less 5nm]	(Chikkaraddy et al., 2018)
	Basic Research (nanoparticle-on-mirror)	Au nanospheres (Au film)	(Cy5) [# integrated in DNA less 5nm]	(Kongsuwan et al., 2018)
Spin coating or dry casting	Basic Research (thermoplasmonic enhancement)	Au nanostars (glass)	~3.5 (NaGd(Y)F4 UCNP)	(Martínez et al., 2018)
Spin coating	Basic Research (single-molecule fluorescence detection)	Au nanorods (ITO glass)	1.5 more total photons (mCherry)	(Donehue et al., 2014)
	Basic Research (optimize spacer distance)	Au nanorods (glass)	3.4-fold (mCherry), 1.5-fold (Cy3.5) [polyelectrolytes, silica ~ 10 nm]	(Fu et al., 2015)
	Basic Research (two photon enhancement of QDs in solution)	Au nanorods (glass)	(CdSe/ZnS core–shell QDs)	(W. Zhang et al., 2018)
	Biosensor (SPCE platform to detect Spermidine)	Au-decorated SiO2A NP hybrids (Ag film)	88-fold (Rh6G) [#dye doped PVA film 30 nm]	(Bhaskar, Kowshik, et al., 2020)
	Basic Research (SPCE platform)	Au nanospheres and Au nanostars (Ag film)	7-fold (Rh6G) for Au nanospheres; 100-fold (Rh6G) for Au nanostars [#dye doped PVA film 30 nm]	(Bhaskar, Patra, et al., 2020)
	Basic Research (photonic crystal-coupled emission (PCCE) and SPCE platforms)	Au Soret colloids; Nd2O3 nanorods (Ag film - SPCE); (one-dimensional photonic crystal - PCCE)	>360-fold (RhB) in SPCE; >1500-fold (RhB) PCCE platform [#dye doped PVA film 30 nm]	(Bhaskar et al., 2021)
	Biosensor (SPCE platform to detect Mefenamic Acid)	AgAu nanocubes (Ag film)	1300-fold (RhB) [#dye doped PVA film 30 nm]	(Bhaskar et al., 2022)
Interfacial assembly	Cell bioimaging (TIRF/ FRET imaging of live cells)	Au@Ag nanocubes, Au@Ag nanorods, and Au nanorods (glass)	3.4 (BDP-FL), 12.9 (Cy5), 62.1 (IR-800CW); 2.1 (Cy3/Cy5 FRET pair) [PDA 20 nm]	(Hou et al., 2020)
Controlled evaporation self-assembly	Basic Research (DNA molecular beacon optimization)	Au nanorods (glass)	~0.8** (Quasar670 dye) [hairpin ssDNA ~ 16 nm]	(Mei & Tang, 2017)
	Basic Research (enhance emission from UCPL)	Au nanorods (glass)	35-fold ($NaYF_4$:Yb^{3+}, Er^{3+} UCNP) [MoO_3 ~8 nm distance]	(Yin et al., 2016)
Template and capillary self-assembly	Basic Research (enhance emission from UCPL)	Au nanorods (silicon)	1.8-fold simulated ($NaYF_4$:Yb^{3+},Er^{3+} UCNPs) [SiO_2 6 nm]	(Greybush et al., 2014)

5-FAM (5-carboxyfluorescein), AF-680 (AlexaFluor680), FRET (Fluorescence resonance energy transfer), PCCE (Photonic Crystal-Coupled Emission), PDA (polydopamine), PDMS (polydimethylsiloxane), PVA (polyvinylalcohol), Quantum Dots (QDs), Rh6G (Rhodamine 6G), RhB (Rhodamine B), SPCE (Surface plasmon-coupled emission), TIRF (Total internal reflection fluorescence), UCNPs (Upconversion Nanoparticles).

**value from graphic plot, see reference for enhancement factor formula calculation details.

Acknowledgement
This project has received funding from the European Union's Horizon 2020 research and innovation programme under grant agreement No 861950, project POSEIDON. Oscar F. Silvestre acknowledges the support from the Provincial Council of Gipuzkoa under the program Fellows Gipuzkoa.

Disclosure statement
No potential conflict of interest was reported by the authors.

Notes on contributors
Oscar F. Silvestre completed his PhD in 2011 at Cardiff University, UK. He joined in 2012 the NIBIB-National Institutes of Health as an AXA Research Fund postdoctoral fellow, to work on nanoparticle platforms for gene/drug therapy. He then obtained a Marie Curie COFUND postdoctoral fellowship in 2016 at INL - International Iberian Nanotechnology Laboratory, Portugal, expanding his research in nonlinear optical imaging for biosensing. In 2019, he became a Fellow Gipuzkoa at CIC biomaGUNE, Spain, where he gained expertise in the synthesis of colloidal gold nanoparticles, plasmon enhanced fluorescence and their biological applications.

Anish Rao completed his B.Sc. with honours in chemistry in 2013 at Ramjas College in Delhi University (India). He then obtained his MS + PhD (in 2020) from Indian Institute of Science Education and Research (IISER) Pune, India. He worked under the supervision of Dr. Pramod P. Pillai on regulating interparticle interactions for nanoparticle self-assembly with increasing degree of complexity. He then moved to a postdoctoral position on the development of multicomponent nanoparticle self-assemblies for applications in photonic integrated circuits, with Prof. Luis M. Liz-Marzán at CIC biomaGUNE, Spain. He is presently working as a Juan de la Cierva fellow at Centro de Física de Materiales (CSIC-UPV/EHU), Spain.

Luis M. Liz-Marzán is an Ikerbasque Professor at CIC biomaGUNE (BRTA), in San Sebastián (Spain), where he also served as Scientific Director from 2012 to 2020. Luis graduated in chemistry from the University of Santiago de Compostela, was postdoc at Utrecht University and Professor at the University of Vigo (1995–2012), where he currently holds a part-time Professor position. Luis has been visiting professor at various research institutions worldwide and received numerous scientific awards and honors. He is also a member of the Spanish Royal Academy of Sciences, European Academy of Sciences and Academia Europaea. He currently serves as an executive editor at *ACS Nano*, and on the editorial advisory board of several journals including *Science*, *Acc. Mater. Res.* and *Adv. Funct. Mater*. Liz-Marzán is known for his work on the colloidal synthesis and self-assembly of metal nanocrystals, as well as the characterization and application of their plasmonic properties. More recently, his research has broadened into the biomedical applications of plasmonic nanostructures.

ORCID

Oscar F. Silvestre https://orcid.org/0000-0002-3750-4187

Anish Rao https://orcid.org/0000-0001-6083-5622

Luis M. Liz-Marzán https://orcid.org/0000-0002-6647-1353

References

Anger, P., Bharadwaj, P., & Novotny, L. (2006). Enhancement and quenching of single-molecule fluorescence. *Physical Review Letters*, *96*(11), 113002. https://doi.org/10.1103/PhysRevLett.96.113002

Aricò, A. S., Bruce, P., Scrosati, B., Tarascon, J. M., & Van Schalkwijk, W. (2005). Nanostructured materials for advanced energy conversion and storage devices. In *Nature Materials* (Vol. 4, Issue 5, pp. 366–377). Nature Publishing Group. https://doi.org/10.1038/nmat1368

Ashoori, R. C. (1996). Electrons in artificial atoms. In *Nature* (Vol. 379, Issue 6564, pp. 413–419). Macmillan Magazines Ltd. https://doi.org/10.1038/379413a0

Asian, K., Lakowicz, J. R., Szmacinski, H., & Geddes, C. D. (2004). Metal-enhanced fluorescence solution-based sensing platform. *Journal of Fluorescence*, *14*(6), 677–679. https://doi.org/10.1023/B:JOFL.0000047217.74943.5c

Auyeung, E., Li, T. I. N. G., Senesi, A. J., Schmucker, A. L., Pals, B. C., De La Cruz, M. O., & Mirkin, C. A. (2014). DNA-mediated nanoparticle crystallization into Wulff polyhedra. *Nature*, *505*(7481), 73–77. https://doi.org/10.1038/nature12739

Barad, H. N., Kwon, H., Alarcón-Correa, M., & Fischer, P. (2021). Large Area Patterning of Nanoparticles and Nanostructures: Current Status and Future Prospects. In *ACS Nano* (Vol. 15, Issue 4, pp. 5861–5875). American Chemical Society. https://doi.org/10.1021/acsnano.0c09999

Bauch, M., Toma, K., Toma, M., Zhang, Q., & Dostalek, J. (2014). Plasmon-Enhanced Fluorescence Biosensors: A Review. In *Plasmonics* (Vol. 9, Issue 4, pp. 781–799). Springer. https://doi.org/10.1007/s11468-013-9660-5

Baumberg, J. J., Aizpurua, J., Mikkelsen, M. H., & Smith, D. R. (2019). Extreme nanophotonics from ultrathin metallic gaps. *Nature Materials 2019 18:7*, *18*(7), 668–678. https://doi.org/10.1038/s41563-019-0290-y

Bhaskar, S., Das, P., Moronshing, M., Rai, A., Subramaniam, C., Bhaktha, S. B. N., & Ramamurthy, S. S. (2021). Photoplasmonic assembly of dielectric-metal, Nd2O3-Gold soret nanointerfaces for dequenching the luminophore emission. *Nanophotonics*, *10*(13), 3417–3431. https://doi.org/10.1515/nanoph-2021-0124

Bhaskar, S., Kowshik, N. C. S. S., Chandran, S. P., & Ramamurthy, S. S. (2020). Femtomolar Detection of Spermidine Using Au Decorated SiO2 Nanohybrid on Plasmon-Coupled Extended Cavity Nanointerface: A Smartphone-Based Fluorescence Dequenching Approach. *Langmuir*, *36*(11), 2865–2876. https://doi.org/10.1021/acs.langmuir.9b03869

Bhaskar, S., Patra, R., Kowshik, N. C. S. S., Ganesh, K. M., Srinivasan, V., Chandran S, P.,

& Ramamurthy, S. S. (2020). Nanostructure effect on quenching and dequenching of quantum emitters on surface plasmon-coupled interface: A comparative analysis using gold nanospheres and nanostars. *Physica E: Low-Dimensional Systems and Nanostructures*, *124*, 114276. https://doi.org/10.1016/j.physe.2020.114276

Bhaskar, S., Rai, A., Ganesh, K. M., Reddy, R., Reddy, N., & Ramamurthy, S. S. (2022). Sericin-Based Bio-Inspired Nano-Engineering of Heterometallic AgAu Nanocubes for Attomolar Mefenamic Acid Sensing in the Mobile Phone-Based Surface Plasmon-Coupled Interface. *Langmuir*, *38*(39), 12035–12049. https://doi.org/10.1021/acs.langmuir.2c01894

Bishop, K. J. M., Wilmer, C. E., Soh, S., & Grzybowski, B. A. (2009). Nanoscale forces and their uses in self-assembly. In *Small* (Vol. 5, Issue 14, pp. 1600–1630). John Wiley & Sons, Ltd. https://doi.org/10.1002/smll.200900358

Boles, M. A., Engel, M., & Talapin, D. V. (2016). *Self-Assembly of Colloidal Nanocrystals: From Intricate Structures to Functional Materials*. https://doi.org/10.1021/acs.chemrev.6b00196

Boneschanscher, M. P., Evers, W. H., Qi, W., Meeldijk, J. D., Dijkstra, M., & Vanmaekelbergh, D. (2013). Electron tomography resolves a novel crystal structure in a binary nanocrystal superlattice. *Nano Lett.*, *13*(3), 1312–1316. https://doi.org/10.1021/nl400100c

Brodin, J. D., Auyeung, E., & Mirkin, C. A. (2015). DNA-mediated engineering of multicomponent enzyme crystals. *Proceedings of the National Academy of Sciences of the United States of America*, *112*(15), 4564–4569. https://doi.org/10.1073/pnas.1503533112

Chekini, M., Filter, R., Bierwagen, J., Cunningham, A., Rockstuhl, C., & Bürgi, T. (2015). Fluorescence enhancement in large-scale self-assembled gold nanoparticle double arrays. *Journal of Applied Physics*, *118*(23), 233107. https://doi.org/10.1063/1.4938025

Chikkaraddy, R., de Nijs, B., Benz, F., Barrow, S. J., Scherman, O. A., Rosta, E., Demetriadou, A., Fox, P., Hess, O., & Baumberg, J. J. (2016). Single-molecule strong coupling at room temperature in plasmonic nanocavities. *Nature*, *535*(7610), 127–130. https://doi.org/10.1038/nature17974

Chikkaraddy, R., Turek, V. A., Kongsuwan, N., Benz, F., Carnegie, C., Van De Goor, T., De Nijs, B., Demetriadou, A., Hess, O., Keyser, U. F., & Baumberg, J. J. (2018). Mapping Nanoscale Hotspots with Single-Molecule Emitters Assembled into Plasmonic Nanocavities Using DNA Origami. *Nano Letters*, *18*(1), 405–411. https://doi.org/10.1021/acs.nanolett.7b04283

Ciracì, C., Hill, R. T., Mock, J. J., Urzhumov, Y., Fernández-Domínguez, A. I., Maier, S. A., Pendry, J. B., Chilkoti, A., & Smith, D. R. (2012). Probing the ultimate limits of plasmonic enhancement. *Science*, *337*(6098), 1072–1074. https://doi.org/10.1126/science.1224823

Cui, Y., Björk, M. T., Liddle, J. A., Sönnichsen, C., Boussert, B., & Alivisatos, A. P. (2004). Integration of colloidal nanocrystals into lithographically patterned devices. *Nano Lett.*, *4*(6), 1093–1098. https://doi.org/10.1021/nl049488i

Daniel, M. C., & Astruc, D. (2004). Gold Nanoparticles: Assembly, Supramolecular Chemistry, Quantum-Size-Related Properties, and Applications Toward Biology, Catalysis, and Nanotechnology. In *Chem.Rev.* (Vol. 104, Issue 1, pp. 293–346). https://doi.org/10.1021/cr030698+

Deegan, R. D., Bakajin, O., Dupont, T. F., Huber, G., Nagel, S. R., & Witten, T. A. (1997). Capillary flow as the cause of ring stains from dried liquid drops. *Nature*, *389*(6653), 827–829. https://doi.org/10.1038/39827

Donehue, J. E., Wertz, E., Talicska, C. N., & Biteen, J. S. (2014). Plasmon-Enhanced

brightness and photostability from single fluorescent proteins coupled to gold nanorods. *Journal of Physical Chemistry C*, *118*(27), 15027–15035. https://doi.org/10.1021/jp504186n

Dong, J., Gao, W., Han, Q., Wang, Y., Qi, J., Yan, X., & Sun, M. (2019). Plasmon-enhanced upconversion photoluminescence: Mechanism and application. *Reviews in Physics*, *4*, 100026. https://doi.org/10.1016/J.REVIP.2018.100026

Dong, J., Zhang, Z., Zheng, H., & Sun, M. (2015). Recent Progress on Plasmon-Enhanced Fluorescence. *Nanophotonics*, *4*(1), 472–490. https://doi.org/10.1515/nanoph-2015-0028

Feng, A. L., Lin, M., Tian, L., Zhu, H. Y., Guo, H., Singamaneni, S., Duan, Z., Lu, T. J., & Xu, F. (2015). Selective enhancement of red emission from upconversion nanoparticles via surface plasmon-coupled emission. *RSC Advances*, *5*(94), 76825–76835. https://doi.org/10.1039/c5ra13184g

Feng, A. L., You, M. L., Tian, L., Singamaneni, S., Liu, M., Duan, Z., Lu, T. J., Xu, F., & Lin, M. (2015). Distance-Dependent Plasmon-Enhanced Fluorescence of Upconversion Nanoparticles using Polyelectrolyte Multilayers as Tunable Spacers. *Scientific Reports 2015 5:1*, *5*(1), 1–10. https://doi.org/10.1038/srep07779

Flauraud, V., Mastrangeli, M., Bernasconi, G. D., Butet, J., Alexander, D. T. L., Shahrabi, E., Martin, O. J. F., & Brugger, J. (2017). Nanoscale topographical control of capillary assembly of nanoparticles. *Nat. Nanotechnol.*, *12*(1), 73–80. https://doi.org/10.1038/nnano.2016.179

Fort, E., & Grésillon, S. (2007). Surface enhanced fluorescence. *Journal of Physics D: Applied Physics*, *41*(1), 013001. https://doi.org/10.1088/0022-3727/41/1/013001

Fu, B., Flynn, J. D., Isaacoff, B. P., Rowland, D. J., & Biteen, J. S. (2015). Super-Resolving the Distance-Dependent Plasmon-Enhanced Fluorescence of Single Dye and Fluorescent Protein Molecules. *Journal of Physical Chemistry C*, *119*(33), 19350–19358. https://doi.org/10.1021/acs.jpcc.5b05154

Gao, W., Emaminejad, S., Nyein, H. Y. Y., Challa, S., Chen, K., Peck, A., Fahad, H. M., Ota, H., Shiraki, H., Kiriya, D., Lien, D. H., Brooks, G. A., Davis, R. W., & Javey, A. (2016). Fully integrated wearable sensor arrays for multiplexed in situ perspiration analysis. *Nature*, *529*(7587), 509–514. https://doi.org/10.1038/nature16521

García-Astrain, C., Lenzi, E., Jimenez de Aberasturi, D., Henriksen-Lacey, M., Binelli, M. R., Liz-Marzán, L. M., García-Astrain, C., Lenzi, E., Jimenez de Aberasturi, D., Henriksen-Lacey, M., Liz-Marzán, L. M., & Binelli, M. R. (2020). 3D-Printed Biocompatible Scaffolds with Built-In Nanoplasmonic Sensors. *Advanced Functional Materials*, *30*(45), 2005407. https://doi.org/10.1002/ADFM.202005407

García-Lojo, D., Núñez-Sánchez, S., Gómez-Graña, S., Grzelczak, M., Pastoriza-Santos, I., Pérez-Juste, J., & Liz-Marzán, L. M. (2019). Plasmonic Supercrystals. *Accounts of Chemical Research*, *52*(7), 1855–1864. https://doi.org/10.1021/acs.accounts.9b00213

Geddes, C. D., & Lakowicz, J. R. (2002). Metal-Enhanced Fluorescence. *Journal of Fluorescence*, *12*(2), 121–129. https://doi.org/10.1023/A:1016875709579/METRICS

Goßler, F. R., Steiner, A. M., Stroyuk, O., Raevskaya, A., & König, T. A. F. (2019). Active Plasmonic Colloid-to-Film-Coupled Cavities for Tailored Light-Matter Interactions. *Journal of Physical Chemistry C*, *123*(11), 6745–6752. https://doi.org/10.1021/acs.jpcc.8b12566

Greybush, N. J., Saboktakin, M., Ye, X., Della Giovampaola, C., Oh, S. J., Berry, N. E., Engheta, N., Murray, C. B., & Kagan, C. R. (2014). Plasmon-enhanced upconversion luminescence in single nanophosphor-nanorod heterodimers formed through template-assisted self-assembly. *ACS Nano*, *8*(9), 9482–9491. https://doi.org/10.1021/nn503675a

Grzelczak, M., Liz-Marzán, L. M., & Klajn, R. (2019). Stimuli-responsive self-assembly of nanoparticles. In *Chemical Society Reviews* (Vol. 48, Issue 5, pp. 1342–1361). The

Royal Society of Chemistry. https://doi.org/10.1039/c8cs00787j
Hamon, C., & Liz-Marzán, L. M. (2015). Hierarchical Assembly of Plasmonic Nanoparticles. *Chemistry – A European Journal*, *21*(28), 9956–9963. https://doi.org/10.1002/CHEM.201500149
Hanske, C., Hill, E. H., Vila-Liarte, D., González-Rubio, G., Matricardi, C., Mihi, A., & Liz-Marzán, L. M. (2019). Solvent-Assisted Self-Assembly of Gold Nanorods into Hierarchically Organized Plasmonic Mesostructures. *ACS Applied Materials and Interfaces*, *11*(12), 11763–11771. https://doi.org/10.1021/acsami.9b00334
He, J., Zheng, W., Ligmajer, F., Chan, C. F., Bao, Z., Wong, K. L., Chen, X., Hao, J., Dai, J., Yu, S. F., & Lei, D. Y. (2017). Plasmonic enhancement and polarization dependence of nonlinear upconversion emissions from single gold nanorod@SiO2@CaF2:Yb3+, Er3+ hybrid core-shell-satellite nanostructures. *Light: Science and Applications*, *6*(5), e16217–e16217. https://doi.org/10.1038/lsa.2016.217
Hou, S., Chen, Y., Lu, D., Xiong, Q., Lim, Y., & Duan, H. (2020). A Self-Assembled Plasmonic Substrate for Enhanced Fluorescence Resonance Energy Transfer. *Advanced Materials*, *32*(8), 1906475. https://doi.org/10.1002/ADMA.201906475
Hueckel, T., Hocky, G. M., Palacci, J., & Sacanna, S. (2020). Ionic solids from common colloids. *Nature*, *580*(7804), 487–490. https://doi.org/10.1038/s41586-020-2205-0
Hueckel, T., Hocky, G. M., & Sacanna, S. (2021). Total synthesis of colloidal matter. In *Nature Reviews Materials* (Vol. 6, Issue 11, pp. 1053–1069). https://doi.org/10.1038/s41578-021-00323-x
Jones, M. R., Seeman, N. C., & Mirkin, C. A. (2015). Programmable materials and the nature of the DNA bond. In *Science* (Vol. 347, Issue 6224). American Association for the Advancement of Science. https://doi.org/10.1126/science.1260901
Joyce, C., Fothergill, S. M., & Xie, F. (2020). Recent advances in gold-based metal enhanced fluorescence platforms for diagnosis and imaging in the near-infrared. In *Materials Today Advances* (Vol. 7, p. 100073). Elsevier. https://doi.org/10.1016/j.mtadv.2020.100073
Kalsin, A. M., Fialkowski, M., Paszewski, M., Smoukov, S. K., Bishop, K. J. M., & Grzybowski, B. A. (2006). Electrostatic self-assembly of binary nanoparticle crystals with a diamond-like lattice. *Science*, *312*(5772), 420–424. https://doi.org/10.1126/science.1125124
Kim, D. H., Ghaffari, R., Lu, N., & Rogers, J. A. (2012). Flexible and stretchable electronics for biointegrated devices. In *Annual Review of Biomedical Engineering* (Vol. 14, pp. 113–128). https://doi.org/10.1146/annurev-bioeng-071811-150018
Kim, Y., Macfarlane, R. J., Jones, M. R., & Mirkin, C. A. (2016). Materials Science: Transmutable nanoparticles with reconfigurable surface ligands. *Science*, *351*(6273), 579–582. https://doi.org/10.1126/science.aad2212
Klajn, R., Bishop, K. J. M., Fialkowski, M., Paszewski, M., Campbell, C. J., Gray, T. P., & Grzybowski, B. A. (2007). Plastic and moldable metals by self-assembly of sticky nanoparticle aggregates. *Science*, *316*(5822), 261–264. https://doi.org/10.1126/science.1139131
Koh, B., Li, X., Zhang, B., Yuan, B., Lin, Y., Antaris, A. L., Wan, H., Gong, M., Yang, J., Zhang, X., Liang, Y., & Dai, H. (2016). Visible to Near-Infrared Fluorescence Enhanced Cellular Imaging on Plasmonic Gold Chips. *Small*, *12*(4), 457–465. https://doi.org/10.1002/smll.201502182
Kongsuwan, N., Demetriadou, A., Chikkaraddy, R., Benz, F., Turek, V. A., Keyser, U. F., Baumberg, J. J., & Hess, O. (2018). Suppressed Quenching and Strong-Coupling of Purcell-Enhanced Single-Molecule Emission in Plasmonic Nanocavities. *ACS Photonics*, *5*(1), 186–191. https://doi.org/10.1021/acsphotonics.7b00668

Kulakovich, O., Gurinovich, L., Li, H., Ramanenka, A., Trotsiuk, L., Muravitskaya, A., Wei, J., Li, H., Matveevskaya, N., Guzatov, D. V., & Gaponenko, S. (2021). Photostability enhancement of InP/ZnSe/ZnSeS/ZnS quantum dots by plasmonic nanostructures. *Nanotechnology*, *32*(3), 035204. https://doi.org/10.1088/1361-6528/abbdde

Kulakovich, O., Strekal, N., Yaroshevich, A., Maskevich, S., Gaponenko, S., Nabiev, I., Woggon, U., & Artemyev, M. (2002). Enhanced Luminescence of CdSe Quantum Dots on Gold Colloids. *Nano Letters*, *2*(12), 1449–1452. https://doi.org/10.1021/nl025819k

Lakowicz, J. R., Ray, K., Chowdhury, M., Szmacinski, H., Fu, Y., Zhang, J., & Nowaczyk, K. (2008). Plasmon-controlled fluorescence: a new paradigm in fluorescence spectroscopy. *Analyst*, *133*(10), 1308–1346. https://doi.org/10.1039/B802918K

Laramy, C. R., O'Brien, M. N., & Mirkin, C. A. (2019). Crystal engineering with DNA. In *Nature Reviews Materials* (Vol. 4, Issue 3, pp. 201–224). Nature Publishing Group. https://doi.org/10.1038/s41578-019-0087-2

Lee, M. S., Yee, D. W., Ye, M., & MacFarlane, R. J. (2022). Nanoparticle Assembly as a Materials Development Tool. In *Journal of the American Chemical Society* (Vol. 144, Issue 8, pp. 3330–3346). https://doi.org/10.1021/jacs.1c12335

Lee, S., A. M, T., Cho, G., & Lee, J. (2022). Control of the Drying Patterns for Complex Colloidal Solutions and Their Applications. *Nanomaterials (Basel, Switzerland)*, *12*(15). https://doi.org/10.3390/NANO12152600

Li, J. F., Li, C. Y., & Aroca, R. F. (2017). Plasmon-enhanced fluorescence spectroscopy. In *Chem. Soc. Rev* (Vol. 46, Issue 13, pp. 3962–3979). The Royal Society of Chemistry. https://doi.org/10.1039/c7cs00169j

Li, X., Kuznetsova, T., Cauwenberghs, N., Wheeler, M., Maecker, H., Wu, J. C., Haddad, F., & Dai, H. (2017). Autoantibody profiling on a plasmonic nano-gold chip for the early detection of hypertensive. *Proceedings of the National Academy of Sciences of the United States of America*, *114*(27), 7089–7094. https://doi.org/10.1073/pnas.1621457114

Li, X., Pomares, C., Gonfrier, G., Koh, B., Zhu, S., Gong, M., Montoya, J. G., & Dai, H. (2016). Multiplexed anti-toxoplasma IgG, IgM, and IgA assay on plasmonic gold chips: Towards making mass screening possible with dye test precision. *Journal of Clinical Microbiology*, *54*(7), 1726–1733. https://doi.org/10.1128/JCM.03371-15

Li, X., Pomares, C., Peyron, F., Press, C. J., Ramirez, R., Geraldine, G., Cannavo, I., Chapey, E., Levigne, P., Wallon, M., Montoya, J. G., & Dai, H. (2019). Plasmonic gold chips for the diagnosis of Toxoplasma gondii, CMV, and rubella infections using saliva with serum detection precision. *European Journal of Clinical Microbiology and Infectious Diseases*, *38*(5), 883–890. https://doi.org/10.1007/s10096-019-03487-1

Li, Y., Sun, J., Wu, L., Ji, J., Sun, X., & Qian, Y. (2014). Surface-enhanced fluorescence immunosensor using Au nano-crosses for the detection of microcystin-LR. *Biosensors and Bioelectronics*, *62*, 255–260. https://doi.org/10.1016/J.BIOS.2014.06.064

Li, Z., Fan, Q., & Yin, Y. (2022). Colloidal Self-Assembly Approaches to Smart Nanostructured Materials. In *Chemical Reviews* (Vol. 122, Issue 5, pp. 4976–5067). American Chemical Society. https://doi.org/10.1021/acs.chemrev.1c00482

Lin, Q.-Y., Mason, J. A., Li, Z., Zhou, W., O'Brien, M. N., Brown, K. A., Jones, M. R., Butun, S., Lee, B., Dravid, V. P., Aydin, K., & Mirkin, C. A. (2018). Building superlattices from individual nanoparticles via template-confined DNA-mediated assembly. *Science (New York, N.Y.)*, *359*(6376), 669–672. https://doi.org/10.1126/science.aaq0591

Liu, B., Li, Y., Wan, H., Wang, L., Xu, W., Zhu, S., Liang, Y., Zhang, B., Lou, J., Dai, H., & Qian, K. (2016). High Performance, Multiplexed Lung Cancer Biomarker Detection on a Plasmonic Gold Chip. *Advanced Functional Materials*, *26*(44), 7994–8002.

https://doi.org/10.1002/ADFM.201603547
Liu, S. F., Hou, Z. W., Lin, L., Li, F., Zhao, Y., Li, X. Z., Zhang, H., Fang, H. H., Li, Z., & Sun, H. B. (2022). 3D nanoprinting of semiconductor quantum dots by photoexcitation-induced chemical bonding. *Science*, *377*(6610). https://doi.org/10.1126/science.abo5345
Luan, J., Morrissey, J. J., Wang, Z., Derami, H. G., Liu, K. K., Cao, S., Jiang, Q., Wang, C., Kharasch, E. D., Naik, R. R., & Singamaneni, S. (2018). *Add-on plasmonic patch as a universal fluorescence enhancer*. *7*(1), 1–13. https://doi.org/10.1038/s41377-018-0027-8
Macfarlane, R. J. (2021). From Nano to Macro: Thinking Bigger in Nanoparticle Assembly. *Nano Letters*. https://doi.org/10.1021/ACS.NANOLETT.1C02724
Macfarlane, R. J., Jones, M. R., Lee, B., Auyeung, E., & Mirkin, C. A. (2013). Topotactic interconversion of nanoparticle superlattices. *Science*, *341*(6151), 1222–1225. https://doi.org/10.1126/science.1241402
Malikova, N., Pastoriza-Santos, I., Schierhorn, M., Kotov, N. A., & Liz-Marzán, L. M. (2002). Layer-by-Layer Assembled Mixed Spherical and Planar Gold Nanoparticles: Control of Interparticle Interactions. *Langmuir*, *18*(9), 3694–3697. https://doi.org/10.1021/LA025563Y
Martínez, E. D., Urbano, R. R., & Rettori, C. (2018). Thermoplasmonic enhancement of upconversion in small-size doped NaGd(Y)F4 nanoparticles coupled to gold nanostars. *Nanoscale*, *10*(30), 14687–14696. https://doi.org/10.1039/C8NR01639A
Mei, Z., & Tang, L. (2017). Surface-Plasmon-Coupled Fluorescence Enhancement Based on Ordered Gold Nanorod Array Biochip for Ultrasensitive DNA Analysis. *Analytical Chemistry*, *89*(1), 633–639. https://doi.org/10.1021/acs.analchem.6b02797
Min, Y., Akbulut, M., Kristiansen, K., Golan, Y., & Israelachvili, J. (2008). The role of interparticle and external forces in nanoparticle assembly. *Nature Materials*, *7*(7), 527–538. https://doi.org/10.1038/nmat2206
Minopoli, A., Della Ventura, B., Campanile, R., Tanner, J. A., Offenhäusser, A., Mayer, D., & Velotta, R. (2021). Randomly positioned gold nanoparticles as fluorescence enhancers in apta-immunosensor for malaria test. *Mikrochimica Acta*, *188*(3). https://doi.org/10.1007/S00604-021-04746-9
Minopoli, A., Della Ventura, B., Lenyk, B., Gentile, F., Tanner, J. A., Offenhäusser, A., Mayer, D., & Velotta, R. (2020). Ultrasensitive antibody-aptamer plasmonic biosensor for malaria biomarker detection in whole blood. *Nature Communications 2020 11:1*, *11*(1), 1–10. https://doi.org/10.1038/s41467-020-19755-0
Minopoli, A., Scardapane, E., Ventura, B. Della, Tanner, J. A., Offenhäusser, A., Mayer, D., & Velotta, R. (2022). Double-Resonant Nanostructured Gold Surface for Multiplexed Detection. *ACS Applied Materials and Interfaces*, *14*(5), 6417–6427. https://doi.org/10.1021/acsami.1c23438
Mock, J. J., Hill, R. T., Degiron, A., Zauscher, S., Chilkoti, A., & Smith, D. R. (2008). Distance-dependent plasmon resonant coupling between a gold nanoparticle and gold film. *Nano Letters*, *8*(8), 2245–2252. https://doi.org/10.1021/nl080872f
Moskovits, M. (1985). Surface-enhanced spectroscopy. *Reviews of Modern Physics*, *57*(3), 783–826. https://doi.org/10.1103/RevModPhys.57.783
Ngo, T. T., Lozano, G., & Míguez, H. (2022). Enhanced up-conversion photoluminescence in fluoride–oxyfluoride nanophosphor films by embedding gold nanoparticles. *Materials Advances*, *3*(10), 4235–4242. https://doi.org/10.1039/D2MA00068G
Ni, S., Isa, L., & Wolf, H. (2018). Capillary assembly as a tool for the heterogeneous integration of micro- and nanoscale objects. *Soft Matter*, *14*(16), 2978–2995. https://doi.org/10.1039/C7SM02496G
Nirmidas Biotech, I. (n.d.). *Nirmidas Biotech, Inc.* Retrieved December 7, 2022, from https://www.nirmidas.com/

Park, D. J., Zhang, C., Ku, J. C., Zhou, Y., Schatz, G. C., & Mirkin, C. A. (2015). Plasmonic photonic crystals realized through DNA-programmable assembly. *Proceedings of the National Academy of Sciences of the United States of America*, *112*(4), 977–981. https://doi.org/10.1073/PNAS.1422649112

Park, S. C., Fang, J., Biswas, S., Mozafari, M., Stauden, T., & Jacobs, H. O. (2014). A First Implementation of an Automated Reel-to-Reel Fluidic Self-Assembly Machine. *Advanced Materials*, *26*(34), 5942–5949. https://doi.org/10.1002/adma.201401573

Pavelka, O., Dyakov, S., Veselý, J., Fučíková, A., Sugimoto, H., Fujii, M., & Valenta, J. (2021). Optimizing plasmon enhanced luminescence in silicon nanocrystals by gold nanorods. *Nanoscale*, *13*(9), 5045–5057. https://doi.org/10.1039/D1NR00058F

Pelesko, J. A. T., Yorifanc^cirotjp, •, & Htaw Kbit, L. (2007). *Self Assembly : The Science of Things That Put Themselves Together*. https://doi.org/10.1201/9781584886884

Pelton, M., Aizpurua, J., & Bryant, G. (2008). Metal-nanoparticle plasmonics. In *Laser and Photonics Reviews* (Vol. 2, Issue 3, pp. 136–159). John Wiley & Sons, Ltd. https://doi.org/10.1002/lpor.200810003

Pomerantseva, E., Bonaccorso, F., Feng, X., Cui, Y., & Gogotsi, Y. (2019). Energy storage: The future enabled by nanomaterials. In *Science* (Vol. 366, Issue 6468). American Association for the Advancement of Science. https://doi.org/10.1126/science.aan8285

Rao, A., Roy, S., Jain, V., & Pillai, P. P. (2022). Nanoparticle Self-Assembly: From Design Principles to Complex Matter to Functional Materials. *ACS Appl. Mater. Interfaces*. https://doi.org/10.1021/acsami.2c05378

Saboktakin, M., Ye, X., Chettiar, U. K., Engheta, N., Murray, C. B., & Kagan, C. R. (2013). Plasmonic enhancement of nanophosphor upconversion luminescence in Au nanohole arrays. *ACS Nano*, *7*(8), 7186–7192. https://doi.org/10.1021/nn402598e

Samanta, D., Zhou, W., Ebrahimi, S. B., Petrosko, S. H., Mirkin, C. A., Samanta, D., Zhou, W., Petrosko, S. H., Mirkin, C. A., & Ebrahimi, S. B. (2022). Programmable Matter: The Nanoparticle Atom and DNA Bond. *Advanced Materials*, *34*(12), 2107875. https://doi.org/10.1002/ADMA.202107875

Sánchez-Iglesias, A., Aldeanueva-Potel, P., Ni, W., Pérez-Juste, J., Pastoriza-Santos, I., Alvarez-Puebla, R. A., Mbenkum, B. N., & Liz-Marzán, L. M. (2010). Chemical seeded growth of Ag nanoparticle arrays and their application as reproducible SERS substrates. *Nano Today*, *5*(1), 21–27. https://doi.org/10.1016/j.nantod.2010.01.002

Santos, P. J., Gabrys, P. A., Zornberg, L. Z., Lee, M. S., & Macfarlane, R. J. (2021). Macroscopic materials assembled from nanoparticle superlattices. *Nature*, *591*(7851), 586–591. https://doi.org/10.1038/s41586-021-03355-z

Scarabelli, L., Hamon, C., & Liz-Marzán, L. M. (2017). Design and fabrication of plasmonic nanomaterials based on gold nanorod supercrystals. In *Chemistry of Materials* (Vol. 29, Issue 1, pp. 15–25). American Chemical Society. https://doi.org/10.1021/acs.chemmater.6b02439

Scarabelli, L., Vila-Liarte, D., Mihi, A., & Liz-Marzán, L. M. (2021). Templated Colloidal Self-Assembly for Lattice Plasmon Engineering. *Accounts of Materials Research*, *2*(9), 816–827. https://doi.org/10.1021/accountsmr.1c00106

Scriven, L. E. (1988). Physics and Applications of DIP Coating and Spin Coating. *MRS Proceedings*, *121*(1), 717–729. https://doi.org/10.1557/proc-121-717

Semeniak, D., Cruz, D. F., Chilkoti, A., & Mikkelsen, M. H. (2022). Plasmonic Fluorescence Enhancement in Diagnostics for Clinical Tests at Point-of-Care: A Review of Recent Technologies. *Advanced Materials*, 2107986. https://doi.org/10.1002/adma.202107986

Shevchenko, E. V., Talapin, D. V., Kotov, N. A., O'Brien, S., & Murray, C. B. (2006). Structural diversity in binary nanoparticle superlattices. *Nature*, *439*(7072), 55–59. https://doi.org/10.1038/nature04414

Smith, A. M., & Nie, S. (2010). Semiconductor nanocrystals: Structure, properties, and band gap engineering. *Acc. Chem. Res.*, *43*(2), 190–200. https://doi.org/10.1021/AR9001069

Spatz, J. P., Mössmer, S., Hartmann, C., Möller, M., Herzog, T., Krieger, M., Boyen, H. G., Ziemann, P., & Kabius, B. (1999). Ordered Deposition of Inorganic Clusters from Micellar Block Copolymer Films. *Langmuir*, *16*(2), 407–415. https://doi.org/10.1021/LA990070N

Steigerwald, M. L., & Brus, L. E. (1990). Semiconductor Crystallites: A Class of Large Molecules. *Acc. Chem. Res.*, *23*(6), 183–188. https://doi.org/10.1021/ar00174a003

Sugimoto, H., Yashima, S., & Fujii, M. (2018). Hybridized Plasmonic Gap Mode of Gold Nanorod on Mirror Nanoantenna for Spectrally Tailored Fluorescence Enhancement. *ACS Photonics*, *5*(8), 3421–3427. https://doi.org/10.1021/acsphotonics.8b00693

Tabakman, S. M., Chen, Z., Casalongue, H. S., Wang, H., & Dai, H. (2011). A New Approach to Solution Phase Gold Seeding for SERS Substrates. *Small (Weinheim an Der Bergstrasse, Germany)*, *7*(4), 499–505. https://doi.org/10.1002/SMLL.201001836

Tabakman, S. M., Lau, L., Robinson, J. T., Price, J., Sherlock, S. P., Wang, H., Zhang, B., Chen, Z., Tangsombatvisit, S., Jarrell, J. A., Utz, P. J., & Dai, H. (2011). Plasmonic substrates for multiplexed protein microarrays with femtomolar sensitivity and broad dynamic range. *Nature Communications*, *2*(1), 466. https://doi.org/10.1038/ncomms1477

Talapin, D. V., & Murray, C. B. (2005). PbSe nanocrystal solids for n- and p-channel thin film field-effect transistors. *Science*, *310*(5745), 86–89. https://doi.org/10.1126/science.1116703

Talapin, D. V, Engel, M., & Braun, P. V. (2015). *Functional materials and devices by self-assembly*. https://doi.org/10.1557/mrs.2020.252

Theodorou, I. G., Ruenraroengsak, P., Gonzalez-Carter, D. A., Jiang, Q., Yagüe, E., Aboagye, E. O., Coombes, R. C., Porter, A. E., Ryan, M. P., & Xie, F. (2019). Towards multiplexed near-infrared cellular imaging using gold nanostar arrays with tunable fluorescence enhancement. *Nanoscale*, *11*(4), 2079–2088. https://doi.org/10.1039/c8nr09409h

Udayabhaskararao, T., Altantzis, T., Houben, L., Coronado-Puchau, M., Langer, J., Popovitz-Biro, R., Liz-Marzán, L. M., Vukovic, L., Král, P., Bals, S., & Klajn, R. (2017). Tunable porous nanoallotropes prepared by post-assembly etching of binary nanoparticle superlattices. *Science*, *358*(6362), 514–518. https://doi.org/10.1126/science.aan6046

Ullrich, S., Scheeler, S. P., Pacholski, C., Spatz, J. P., & Kudera, S. (2013). Formation of Large 2D Arrays of Shape-Controlled Colloidal Nanoparticles at Variable Interparticle Distances. *Particle & Particle Systems Characterization*, *30*(1), 102–108. https://doi.org/10.1002/PPSC.201200065

Vila-Liarte, D., Feil, M. W., Manzi, A., Garcia-Pomar, J. L., Huang, H., Döblinger, M., Liz-Marzán, L. M., Feldmann, J., Polavarapu, L., & Mihi, A. (2020). Templated-Assembly of CsPbBr3 Perovskite Nanocrystals into 2D Photonic Supercrystals with Amplified Spontaneous Emission. *Angew. Chem. Int.Ed.*, *59*(40), 17750–17756. https://doi.org/10.1002/ANIE.202006152

Vogel, N., Retsch, M., Fustin, C. A., Del Campo, A., & Jonas, U. (2015). Advances in Colloidal Assembly: The Design of Structure and Hierarchy in Two and Three Dimensions. In *Chemical Reviews* (Vol. 115, Issue 13, pp. 6265–6311). American Chemical Society. https://doi.org/10.1021/cr400081d

Wang, J., & Jia, Z. (2018). Metal nanoparticles/porous silicon microcavity enhanced surface plasmon resonance fluorescence for the detection of DNA. *Sensors (Switzerland)*, *18*(2), 661. https://doi.org/10.3390/s18020661

Wang, S., Xu, J., Wang, W., Wang, G. J. N., Rastak, R., Molina-Lopez, F., Chung, J. W.,

Niu, S., Feig, V. R., Lopez, J., Lei, T., Kwon, S. K., Kim, Y., Foudeh, A. M., Ehrlich, A., Gasperini, A., Yun, Y., Murmann, B., Tok, J. B. H., & Bao, Z. (2018). Skin electronics from scalable fabrication of an intrinsically stretchable transistor array. *Nature*, *555*(7694), 83–88. https://doi.org/10.1038/nature25494

Wang, Y., & Ding, T. (2019). Optical tuning of plasmon-enhanced photoluminescence. *Nanoscale*, *11*(22), 10589–10594. https://doi.org/10.1039/C9NR03725J

Wang, Y., Fedin, I., Zhang, H., & Talapin, D. V. (2017). Direct optical lithography of functional inorganic nanomaterials. *Science*, *357*(6349), 385–388. https://doi.org/10.1126/science.aan2958

Whitesides, G. M., & Boncheva, M. (2002). Beyond molecules: Self-assembly of mesoscopic and macroscopic components. *Proc. Natl. Acad. Sci. U.S.A.*, *99*(8), 4769–4774. https://doi.org/10.1073/PNAS.082065899/ASSET/4C112F50-DAEF-4ECA-9891-CA24D2AE82F0/ASSETS/GRAPHIC/PQ0820658002.JPEG

Xie, K. X., Liu, Q., Jia, S. S., & Xiao, X. X. (2021). Fluorescence enhancement by hollow plasmonic assembly and its biosensing application. *Analytica Chimica Acta*, *1144*, 96–101. https://doi.org/10.1016/J.ACA.2020.12.008

Xu, W., Wang, L., Zhang, R., Sun, X., Huang, L., Su, H., Wei, X., Chen, C. C., Lou, J., Dai, H., & Qian, K. (2020). Diagnosis and prognosis of myocardial infarction on a plasmonic chip. *Nature Communications 2020 11:1*, *11*(1), 1–9. https://doi.org/10.1038/s41467-020-15487-3

Yi, C., Liu, H., Zhang, S., Yang, Y., Zhang, Y., Lu, Z., Kumacheva, E., & Nie, Z. (2020). Self-limiting directional nanoparticle bonding governed by reaction stoichiometry. *Science*, *369*(6509), 1369–1374. https://doi.org/10.1126/SCIENCE.ABA8653

Yin, Z., Zhou, D., Xu, W., Cui, S., Chen, X., Wang, H., Xu, S., & Song, H. (2016). Plasmon-Enhanced Upconversion Luminescence on Vertically Aligned Gold Nanorod Monolayer Supercrystals. *ACS Applied Materials & Interfaces*, *8*(18), 11667–11674. https://doi.org/10.1021/acsami.5b12075

Zhang, B., Jarrell, J. A., Price, J. V., Tabakman, S. M., Li, Y., Gong, M., Hong, G., Feng, J., Utz, P. J., & Dai, H. (2013). An Integrated Peptide-Antigen Microarray on Plasmonic Gold Films for Sensitive Human Antibody Profiling. *PLoS ONE*, *8*(7), e71043. https://doi.org/10.1371/journal.pone.0071043

Zhang, B., Kumar, R. B., Dai, H., & Feldman, B. J. (2014). A plasmonic chip for biomarker discovery and diagnosis of type 1 diabetes. *Nature Medicine*, *20*(8), 948–953. https://doi.org/10.1038/nm.3619

Zhang, B., Price, J., Hong, G., Tabakman, S. M., Wang, H., Jarrell, J. A., Feng, J., Utz, P. J., & Dai, H. (2012). Multiplexed cytokine detection on plasmonic gold substrates with enhanced near-infrared fluorescence. *Nano Research 2012 6:2*, *6*(2), 113–120. https://doi.org/10.1007/S12274-012-0286-2

Zhang, W., Caldarola, M., Lu, X., & Orrit, M. (2018). Plasmonic Enhancement of Two-Photon-Excited Luminescence of Single Quantum Dots by Individual Gold Nanorods. *ACS Photonics*, *5*(7), 2960–2968. https://doi.org/10.1021/acsphotonics.8b00306

Zhao, H., Sen, S., Udayabhaskararao, T., Sawczyk, M., Kucanda, K., Manna, D., Kundu, P. K., Lee, J. W., Král, P., & Klajn, R. (2016). Reversible trapping and reaction acceleration within dynamically self-assembling nanoflasks. *Nature Nanotechnology*, *11*(1), 82–88. https://doi.org/10.1038/nnano.2015.256

Zhao, J., Cheng, Y., Shen, H., Hui, Y. Y., Wen, T., Chang, H. C., Gong, Q., & Lu, G. (2018). Light Emission from Plasmonic Nanostructures Enhanced with Fluorescent Nanodiamonds. *Scientific Reports 2018 8:1*, *8*(1), 1–8. https://doi.org/10.1038/s41598-018-22019-z

Zhao, S., Caruso, F., Dahne, L., Decher, G., De Geest, B. G., Fan, J., Feliu, N., Gogotsi, Y.,

Hammond, P. T., Hersam, M. C., Khademhosseini, A., Kotov, N., Leporatti, S., Li, Y., Lisdat, F., Liz-Marzan, L. M., Moya, S., Mulvaney, P., Rogach, A. L., … Parak, W. J. (2019). The Future of Layer-by-Layer Assembly: A Tribute to ACS Nano Associate Editor Helmuth Mohwald. *ACS Nano*, *13*(6), 6151–6169. https://doi.org/10.1021/acsnano.9b03326

Zhao, X., Yang, L., Guo, J., Xiao, T., Zhou, Y., Zhang, Y., Tu, B., Li, T., Grzybowski, B. A., & Yan, Y. (2021). Transistors and logic circuits based on metal nanoparticles and ionic gradients. *Nat. Electronics*, *4*(2), 109–115. https://doi.org/10.1038/s41928-020-00527-z

Graphical abstract